Master's Thesis

Comparison of genomes and host interactions of *Finnlakeviridae* phages

Kim Kreuze

University of Jyväskylä

Department of Biological and Environmental Science

15 May 2023

UNIVERSITY OF JYVÄSKYLÄ, Faculty of Mathematics and Science
Department of Biological and Environmental Science
Master's Degree Programme in Cell and Molecular Biology

Kreuze, Kim	Comparison of genomes and host interactions of *Finnlakeviridae* phages
MSci Thesis	45 p., 5 appendices (8 p.)
Supervisors:	Professor Lotta-Riina Sundberg, PhD Elina Laanto, Doctoral Researcher Kati Mäkelä
Tarkastajat:	PhD Cindy Given, PhD Docent Matti Jalasvuori
May 2023	

Keywords: Diversity, environment, *Finnlakevirus FLiP*, holin-endolysin, lake, myophage, plaque morphology, single-stranded DNA, transient

Bacteriophages containing both a lipid membrane and single-stranded DNA are a novel and highly understudied group despite new isolates and genetic signatures being discovered around the world. FLiP, the sole phage isolate in the family *Finnlakeviridae*, was the first phage characterized with such properties and has an unusual life cycle. The aim of this thesis was to describe two newly isolated bacteriophages (one being similar to FLiP) from lake Jyväsjärvi and compare their host interactions with FLiPs to understand the diversity of *Finnlakeviridae* phages and confirm FLiPs unusual life cycle. To explore the phylogeny and genomic characteristics of both bacteriophages, their genomes were assembled, annotated, and analysed using a variety of bioinformatic software. In addition, phage-host interactions were studied by adsorption assay, one step growth curve, host range assay and zymography. Morphology of the bacteriophages was determined using transmission electron microscopy. Genome assembly of one of the phages revealed it to have a 96.64% nucleotide identity to FLiP and was named FLiP-2. Non-synonymous codon differences between FLiP and FLiP-2 in ORFs with functions related to peptidoglycan degradation and putative receptor binding were found. Additionally, FLiP and FLiP-2 were shown to have slightly different host ranges, plaque morphologies and potential differences in lytic enzyme activity. The second phage was determined to be a tailed bacteriophage with a myophage morphology and was named B330-P19. It was shown to have a highly different host range and plaque morphology compared to both FLiP phages. Finally, the one step growth curve revealed that the three phages differed by their calculated average burst size which was 4.58, 2.63 and 27.73 for FLiP, FLiP-2 and B330-P19 respectively. The results expand the known diversity of *Finnlakevirus FLiP*, the species encompassing FLiP and FLiP-2, and shows that the species is established either in lake Jyväsjärvi, the surrounding environment or both. Additionally, the unusual lifestyle of FLiP seems to be a trait of at least the species and can be different from some tailed phages infecting the same host.

JYVÄSKYLÄN YLIOPISTO, Matemaattis-luonnontieteellinen tiedekunta
Bio- ja ympäristötieteiden laitos
Solu- ja molekyylibiologian maisteriohjelma

Kreuze, Kim	*Finnlakeviridae*– faagien genomien ja isäntä vuorovaikutusten vertailu
Pro gradu tutkielma:	45 s., 5 liitettä (8 s.)
Työn ohjaajat:	Professori Lotta-Riina Sundberg, filosofian tohtori Elina Laanto, väitöskirjatutkija Kati Mäkelä
Tarkastajat:	Filosofian tohtori Cindy Given, filosofian tohtori dosentti Matti Jalasvuori
Toukokuu 2023	

Hakusanat: *Finnlakevirus FLiP*, holiini-endolysiini, järvi, monimuotoisuus, myofaagi, plakkimorfologia, ympäristö, yksijuosteinen DNA, vaihteleva

Faagit, jotka sisältävät lipidikalvon sekä yksijuosteista DNA:ta (ssDNA) ovat vähemmän tutkittuja verrattuna hännällisiin kaksijuosteisiin DNA- (dsDNA) faageihin, vaikka uusia ssDNA isolaatteja sekä geneettisiä signaaleja on alettu löytää ympäri maailmaa. FLiP oli ensimmäinen karakterisoitu faagi, jolla on nämä ominaisuudet, ja toistaiseksi ainoa *Finnlakeviridae* -virusperheen edustaja. Tutkielman tavoite oli karakterisoida kahta vuonna 2021 eristettyä faagi-isolaattia (ss- ja dsDNA sisältäviä) jotka infektoivat samoja Flavobakteeri- isäntiä kuin FLiP. Lisäksi haluttiin verrata FLiP -faagin ja uusien faagien isäntävuorovaikutusdynamiikkoja. Molempien bakteriofagien genomit koottiin, annotoitiin sekä analysoitiin useita eri bioinformaattisia ohjelmia käyttäen. Myös faagien isäntäkirjoja, adsorptiokäyriä, kasvukäyriä ja zymogrammeja verrattiin. Bakteriofagien morfologiaa tarkasteltiin läpäisyelektronimikroskoopilla. FLiP -faagin ja uuden ssDNA -faagin geneettinen vertailu osoitti, että niiden genomisekvenssien samankaltaisuus oli 96.64%, ja faagin nimeksi annettiin FLiP-2 tässä tutkielmassa. Nuklelotidierot kohdistuivat muun muassa viruksen koodittamaan hypoteettiseen piikkiproteiiniin ja proteiineihin, joilla on peptidoglykaanin pilkkomis- kyky. Lisäksi eroja löytyi faagien plakkikoossa, isäntäkirjossa ja mahdollisesti peptidoglykaanin pilkkomiskyvyssä. DsDNA -faagin osoitettiin olevan hännällinen myofaagi, ja sen nimeksi tuli B330-P19. Tämän faagin plakkimorfologia ja isäntäkirjo poikkesi suuresti molemmista FLiP -faageista. Lisäksi B330-P19 faagin kasvukäyrä osoitti, että se tuotti keskimäärin 27,73 uutta partikkelia infektoitua solua kohden, kun taas FLiP ja FLiP-2 faagien kohdalla vastaavat arvot olivat 4,58 ja 2,63. Tulokset laajentavat tunnettua Finnlakeviridae -perheen monimuotoisuutta ja osoittavat, että *Finnlakeviridae* faagit lisääntyvät joko Jyväsjärvessä tai sen ympäristössä. Lisäksi FLiP -faagin erikoisen elinkaaren kaltaisia elinkaarta ei esiinny hännällisellä faagilla, joka kuitenkin infektoi samoja isäntiä.

TABLE OF CONTENTS

TERMS AND ABBREVIATIONS

Terms

FLiP	First phage isolate of the species *Finnlakevirus FLiP*
FLiP-2	Second phage isolate of the species *Finnlakevirus FLiP*
Finnlakevirus FLiP	Bacteriophage species
Muralytic	Synonym for peptidoglycan degrading
Virion	Infective virus particle outside the cell
Plaque	Small circular, cleared area in a cell lawn caused by infection of one or more virions.
Titer	Refers to the concentration of infectious phage particles in a solution usually measured in PFU/ml
Lysis	Rupture and death of a cell
Capsid	Protein shell surrounding virus genome
Tail	The extension protruding out of capsids through which tailed phages eject their genomes
Baseplate	Structure, made of several proteins at the base of tailed phages that is usually thicker than the tail
Burst size	The average number of phages that are released per infected cell
Latent period	The period between initial infection and phage release with cell lysis
Burst period	The period when the phages are released from infected cells with lysis, increasing the titers
Plateau	The period when the titer increase stops, signaling the end of the burst period

Abbreviations

SDS-PAGE	Sodium dodecyl sulphate- protein agarose gel electrophoresis, a method to separate proteins by molecular weight
PFU	Plaque forming unit, the units used to count plaques
MOI	Multiplicity of infection, the ratio of phage particles to host cells after mixing them together
dsDNA	double stranded DNA
ssDNA	single stranded DNA
ORF	Open reading frame
rpm	Rounds per minute
RT	Room temperature
LB	Lysogeny broth or Luria-Bertani
HTC	High Tryptone Cytophaga

BLAST	Basic local alignment search tool

1 INTRODUCTION

Bacteriophages (phages) are viruses that specifically infect bacteria. As viruses, phages are obligate intracellular parasites consisting of a genome surrounded by a protein shell (capsid) and/or lipid membrane. Viruses are thought to be among the most abundant biological units on earth, approximating at 10^{31} particles (Hendrix et al. 1999; Mushegian 2020). Hence, they are thought to be contributing agents in the global carbon cycle (Fuhrman 1999). In addition to having ecological contributions, they are also important in modulating health of multicellular organisms by directly affecting their microbiome (Zuppi et al. 2022). Being the central study models during the molecular biology revolution in the last century, their study has been instrumental to developing experimental antimicrobial drugs (Lin et al. 2017; Sioud 2019) and tools for biotechnology (Vandamme and Mortelmans 2019; Sioud 2019). Additionally, the growing increase of antimicrobial resistance (AMR) has led to a recent surge in popularity in the west on phage therapy research (Lin et al. 2017). From these limited examples it is clear that bacteriophage ecology and molecular biology need to be studied to be of use.

1.1 Phage life cycles

The life cycle of a phage can be divided into five separate phases: adsorption, entry, transcription and replication, assembly and release. When outside the cell, phage particles (virions) move via Brownian motion until they attach to a surface receptor of their host bacteria in a process termed adsorption (Rakhuba et al. 2010). For most phages there is first primary, reversible adsorption phase where they are weakly attached to a host cell. After weakly binding to the host cell, they find the main host receptor and attach irreversibly starting the next part of their life cycle (Anderson 1949; Moldovan et al. 2007; Storms and Sauvageau 2015; Gong et al. 2021). The majority of described phages start the entry phase of their life cycles after irreversible adsorption by injecting their genomes into the host cell by different mechanisms (Rakhuba et al. 2010). To do this, several but not all phages have to locally degrade the peptidoglycan layer that forms part of the bacterial cell wall with a group of enzymes called peptidoglycan hydrolases, which they carry in or on the virion (Rakhuba et al. 2010; Fernandes and São-José 2018). After entry, the released phage genome can either start the next phase by expressing specific genes and replicating or just stay latent inside its host. During active replication and expression, the host is manipulated into producing more copies of the phage genome and transcribing both host and phage genes that directly benefit phage reproduction. One of the most important group of genes expressed produce structural proteins that package the replicated genomes to form new virus particles in a process called assembly. The final stage in the virus life cycle is virus particle release which is often managed by the timed lysis of the host bacteria (Fernandes and São-José 2018). The larger double-stranded (ds)

DNA phages mostly rely on a holin-endolysin system where peptidoglycan degrading enzymes like endolysins accumulate in the cytoplasm or periplasm until holin proteins make holes in the inner bacterial cell membrane so that the endolysins can degrade the peptidoglycan (Catalão et al. 2013; Fernandes and São-José 2018; Zhang et al. 2022). The smaller genome containing ssDNA phages typically rely on a single-gene system with peptidoglycan synthesis inhibiting or peptidoglycan degrading enzymes (Roux et al. 2012; Chamakura and Young 2019). Due to the characteristic lysis of the cell at the end, this is called the lytic life cycle.

Although most phage life cycles follow the basic principles of the lytic cycle, other life cycles are also apparent. The classic, alternative is known as lysogenic life cycle and those that perform this are called temperate phages. Instead of immediately replicating after genome entry and quickly causing lysis, the lysogenic life cycle consists of the phage genome becoming a latent prophage, either integrated to the host genome (Lederberg and Lederberg 1953; Hayashi et al. 1990; Lunde et al. 2003) or as a plasmid in the cytoplasm (Sternberg and Austin 1981; Eggers and Samuels 1999). There the phage replicates together with the host without causing major harm and in some cases even providing selective advantages to the host (Wang et al. 2010). Despite being benign for a time, most temperate phages also cause lysis after certain criteria are met. These two life cycles are currently the most well understood and are found to be used by phages from different taxa.

A consequence of the frequently lytic nature of phage infections is that they can cause small clear areas (called plaques) on a layer of bacterial growth (called lawn). Plaques can have a large variety of different sizes, opacities and nuanced shapes which depend on biological and physical properties of the phage, surface and host (Abedon and Yin 2009; Gallet et al. 2011). Biological factors affecting the plaque size are for example the burst size (i.e. how many phages are produced per bacteria) and latent period (i.e. the time between infection an phage release). Although exceptions are known to exist (e.g. Gallet et al. 2011), it is thought that larger burst sizes and shorter latent periods generally would lead to larger plaques (Yin and McCaskill 1992; Abedon et al. 2003; Abedon and Culler 2007a, b). However, the size and shape of the phage together with agar percentage on the plate and media also has an effect as larger, more unevenly shaped phage particles do not diffuse as well through the agar than smaller, evenly shaped ones (Yin and McCaskill 1992; Gallet et al. 2011). Due to the various factors affecting plaque morphology it is difficult to compare phages by plaque morphology alone but can still prove valuable to differentiate them to some extent.

1.2 Virus taxonomy

Virus taxonomy is complex and has recently been revised by the international committee of taxonomy on viruses (ICTV, Turner et al. 2023). The reason for this complexity is the lack of universal marker genes like the 16s rDNA found in most bacteria. Regardless, some relatedness can be inferred by the presence of certain

genes, so-called virus hallmark genes (VHGs), that are found in only some taxa and not others indicating relatedness (Koonin et al. 2020). These conserved genes typically encode for proteins that are of vital importance to viral life cycles like RNA-dependent RNA polymerases (RdRP) for RNA viruses or structural proteins like the major capsid proteins (MCPs). Utilizing these criteria, bacteriophages with dsDNA genomes are divided among two officially recognized realms, a taxonomic level comparable to the domain level in cellular organisms. The two-bacteriophage containing dsDNA virus realms are Duplodnaviria and Varidnaviria (Figure 1).

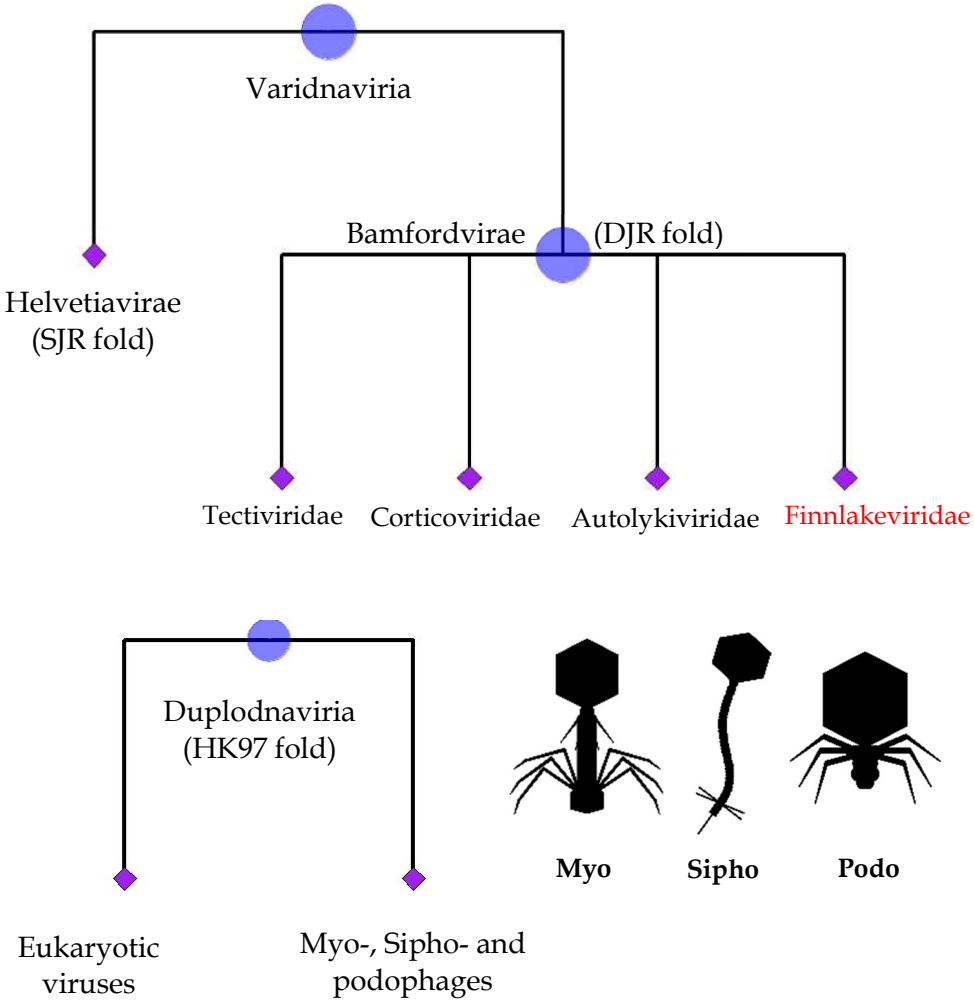

Figure 1. Taxonomic tree showing the two-dsDNA bacteriophage containing realms and the relevant taxa with some descriptions. All taxa in these two kingdoms are dsDNA based except for the member of the family Finnlakeviridae highlighted in red. On the right of the Myo-, Sipho- and podophages clade, the silhouettes of each phage type is presented as a reference to their morphology. Tree was adapted from Koonin et al. (2020). The silhouettes were downloaded from PhyloPic R package website.

1.2.1 Duplodnaviria and tailed phages

The realm Duplodnaviria is mainly characterized by bacteriophages that have a very specific fold in their MCPs called an HK97 fold. All the viruses within this realm contain a dsDNA genome. Additionally, a prominent morphological feature in most of the phages in this large taxon is that they have a tail attached to the capsid. Bacteriophage tails come in a large variety of shapes and sizes, traits that are used to classify them as having myo-, sipho- or podophage morphology (Figure 1, bottom right). Myophages, are characterized by having long tails surrounded by thick and rigid protein sheaths, allowing their tails to contract like syringes, and baseplate structures at the end of the tail. Siphophages are like myophages in their tail lengths and structures but notably lack the protein sheaths and thus have flexible tails. Podophages, on the other hand are characterized by having short non contractile tails that can be hard to differentiate from the capsid in electron microscope images (Fokine and Rossmann 2014). Although previously, tailed bacteriophage phylogeny was defined by the previously mentioned tail morphology, mounting evidence suggests that such a grouping is not favourable as phages of similar tail morphology do not necessarily have more genetic relatedness (Rohwer and Edwards 2002; Aiewsakun et al. 2018; Turner et al. 2023). Thus, tailed bacteriophages are currently classified throughout hundreds of different high-order taxa within the class *Caudoviricetes* and can have surprisingly little sequence homology between each other (Turner et al. 2023).

On a molecular level, tailed bacteriophages have been documented to have genome sizes ranging from 11 kilo base pairs (kbp) all the way to about 735 kbp (Zhou et al. 1995; Al-Shayeb et al. 2020), carrying information on evolutionarily conserved structural proteins to accessory genes with no known function. One such group of paired conserved proteins are the two terminase subunits which are essential multifunctional proteins that pack the phage genome into the fully formed capsid before attaching the tail (Rao and Feiss 2008; Fokine and Rossmann 2014; Black 2015). Tailed phages can also encode non-structural proteins such as tRNAs which allow them to assimilate cell resources more efficiently by using its own optimisied tRNA rather than the bacterium's (Weiss et al. 1968; Bailly-Bechet et al. 2007). Some of the tailed phages with larger genomes also encode CRISPR spacers and Cas proteins, parts of a bacterial immune system, although these are so far rare and hence not too much is known for certain about their functions (Al-Shayeb et al. 2022).

In addition to being a diverse lineage, tailed bacteriophages form a disproportionately large majority of the isolated bacteriophages, with over 80% of isolated bacteriophages belonging to this taxon in 2016 (Székely and Breitbart 2016). Although this may be indicative of the success of tailed bacteriophages relative to others, metagenomic analyses reveal that this difference in isolation may only be a sampling artefact or a product of mostly isolating phages with limited model bacteria (Székely and Breitbart 2016; Kauffman et al. 2018; Mäntynen et al. 2019). Given this vast overrepresentation of tailed phage isolates

they are also the most studied group of phages which is more of a reason to find and characterize phages of different lineages and morphologies.

1.2.2 Varidnaviria and lipid containing phages

Like the Duplodnaviria, the realm of Varidnaviria is mostly composed of dsDNA bacteriophages and has viruses with similar protein folds in their MCPs. However, Varidnaviria contains two lineages at the kingdom level that have slight differences in their MCP folds. The kingdom Bamfordvirae, is defined by having a double jellyroll (DJR) fold while members of the kingdom Helvetiavirae have MCPs with a single jellyroll (SJR) fold (Santos-Pérez et al. 2019; Koonin et al. 2020). All bacteriophages in Varidnaviria belong to Bamfordvirae and are separated into four families called Tectiviridae, Corticoviridae, Autolykiviridae and Finnlakeviridae, the last of which will be discussed in more detail in section 1.4. One of the interesting features that these bacteriophages share is that they contain a lipid membrane on the inside of their capsids which makes them sensitive to detergents and chloroform.

The first Tectiviridae phage isolated was PRD1, which has a 65 nm diameter capsid and a linear 15 kb dsDNA genome (Olsen et al. 1974; Ackermann et al. 1978). It is a lytic phage that was first isolated from sewage water and is known to infect a wide range of gram-negative bacteria carrying specific plasmids (i.e. plasmid dependent) (Olsen et al. 1974). The presence of an internal lipid membrane and early discovery has made PRD1 a model system to study protein-lipid interactions. Phages from the family Corticoviridae are similar to PRD1 in that they have a similar structure although the genomes within the lipid membranes are circular dsDNA. The most studied type species of this phage family is PM2 which has a particle diameter of 60 nm and a 10 kb genome (Espejo and Canelo 1968; Espejo et al. 1969). Like PRD1, PM2 is a lytic virus although several PM2-like prophages have been found in metagenomic data indicating other life cycles are also possible (Krupovič and Bamford 2007).

As mentioned previously, a consequence of this lipid membrane inside the capsids is that they are sensitive to chloroform. Given that several phage isolations protocols use chloroform to remove bacteria, it is thought to be one of the reasons why there are so few phage isolates of this type (see Kauffman et al. 2018; Mäntynen et al. 2019). Supporting the view that the few isolates of lipid containing phages may be due to methodology, metagenomics and isolation methods without chloroform have found these phages in great abundance in marine ecosystems and wastewater (Krupovič and Bamford 2007; Kauffman et al. 2018). In fact, Kauffman et al. (2018) isolated a large group of these phages with a capsid size of 50 nm and 10 kb dsDNA genomes that infect bacteria from the family *Vibrionaceae* and were classified to the family, Autolykiviridae, one of the latest phage families to join the realm Varidnaviria.

1.3 The genus *Flavobacterium* and relatives

The genus *Flavobacterium* is a diverse Gram-negative group in the phylum Bacteroidetes. Members of this genus are typically rod-shaped, 2-5 µm long and 0.3 – 0.5 µm wide depending on species and growth conditions (Bernardet and Bowman 2006). Despite the lack of a flagella, several species in this genus have the ability to move by gliding on solid surfaces (termed gliding motility) with the help of a type IX secretion system (McBride and Zhu 2013; Abby et al. 2016). The type IX secretion system of *F. johnsonie* is the most well understood and serves as a model for this form of locomotion (Gorasia et al. 2020).

Although a few of *Flavobacterium* species are pathogenic to fish and cause disease outbreaks in aquaculture settings, most are environmental, non-pathogenic microbes (Bernardet and Bowman 2006). The environmental species are found in freshwater conditions at large abundances and have been shown to periodically increase in numbers during blooms (Eiler and Bertilsson 2007). Perhaps due to their non-pathogenicity however, not much is known about their ecology or function in the environment.

The majority of phages known to infect *Flavobacterium* sp. are dsDNA tailed phages of myo-, sipho- and podophage morphology (Laanto et al. 2011; Nilsson et al. 2020). Most of these phages are lytic although a subset of lysogenic phages has also been identified (Nilsson et al. 2020). Recently, a novel ssDNA phage named Flavobacterium-infecting lipid-containing phage (FLiP) has been isolated (Laanto et al. 2017b).

1.4 FLiP

FLiP is the first ssDNA phage discovered that infects members of the genus *Flavobacterium*. The FLiP genome is 9174 nucleotides (nt) long and encodes for 16 putative open reading frames (ORFs; Figure 2 A). Structurally, it is a 60 nm in diameter icosahedral virus with spikes protruding from the five-fold axes of symmetry that contains a circular genome surrounded by a lipid membrane (Figure 2 B; Laanto et al. 2017b). The combination of lipid membrane and ssDNA genome made FLiP the first described phage of its kind as such a combination was not known in any other phage. In addition, despite having an ssDNA genome, the double jellyroll motif in its MCP places FLiP into the Varidnaviria realm which before only contained dsDNA viruses (Figure 1). Due to this unique combination of characteristics, FLiP was allocated to its own virus family: Finnlakeviridae (Mäntynen et al. 2020), where it remains the sole member with the species name *Finnlakevirus FLiP* (Koonin et al. 2020).

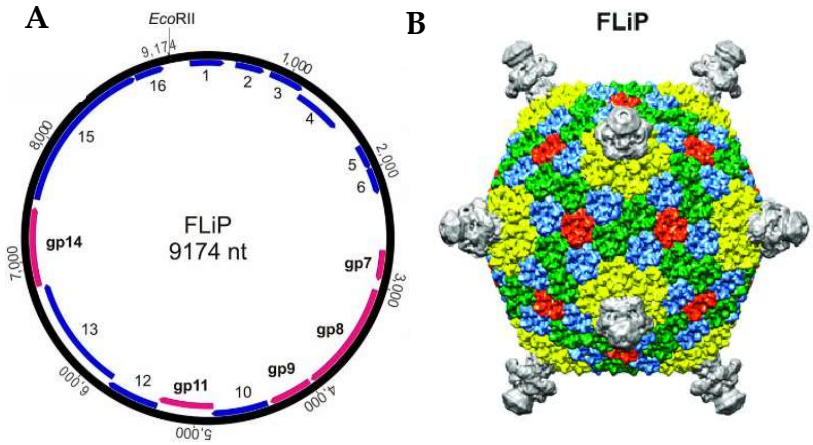

Figure 2. Schematic of FLiP genome and virion. A) FLiP genome is a circular ssDNA of 9174 nt long, 16 ORFs and a single *Eco*RII resctriction site where enumeration starts (Laanto et al. 2017b). The magenta arrows represent confirmed structural proteins and are named GP 7, 8, 9, 11 and 14. The blue arrows are ORFs which have not been confirmed to be structural. B) Virion structure solved by cryo EM illustrating MCP protein trimers in different colors and spike proteins on the 5-fold axes of symmetry. Images were attained from Laanto et al. (2017b).

Reflecting the unique morphology of lipid containing, ssDNA phages, FLiP also has an unusual life cycle that is difficult to study *in vitro*. It infects three different environmental *Flavobacterium* sp. called B330 (original host), B167 and B114 producing clear and sometimes turbid plaques of differing sizes (Marjakangas 2014). In liquid culture however, bacterial growth continues increasing normally after infection while viral titres increase as well (unpublished data). Although this would not be the first bacteriophage with such characteristics *in vitro* (e.g. Shkoporov et al. 2018), it is still considered unusual and would be important to investigate further as it could be related to FLiPs unique combination of traits.

Since the description of FLiP, more studies have pointed to the idea that lipid containing ssDNA phages are more abundant than was previously thought. For example, the Cellulophaga phage phi48:2 has slight protein homology to FLiP MCP (Yutin et al. 2018) and recent evidence suggests it contains an internal lipid membrane (Assimakopolou 2022). Recently, a temperate bacteriophage called phiCjT-23 was structurally described and shown to have a ssDNA genome, lipid membrane and slight sequence homology to FLiP and PM2 (Kejzar et al. 2022). More importantly, sequences belonging to phiCjT-23 produces hits to several bacterial sequences isolated from 5 different continents likely indicating that these types of phages are ubiquitous (Kejzar et al. 2022). This is important as this means a large group of phage diversity has not been characterized and almost nothing is known about them. Clearly, the unusual aspects of FLiP coupled to the potential abundance of this group of phages around the world warrants further basic research as it could provide insight into viral ecology, evolution and understanding to new molecular biology mechanisms. There may even be potential to develop FLiP to become a tool for phage therapy by artificially increasing the host range as was done by Mäkelä (2019).

In the autumn of 2021, two new phages were isolated from lake Jyväsjärvi that infect the same *Flavobacterium* isolates as FLiP: B114, B167 and B330. Preliminary analysis indicated that one of the phages was a non-lipid containing virus which was hypothesised to be a tailed phage and called B330-P19. This newly isolated phage could serve as a good control to study the unique properties of FLiPs life cycle. The other phage was chloroform sensitive and only had a few nucleotide differences in a portion of the MCP gene (i.e. GP8) compared to FLiP which is why it was given the name FLiP-2. This phage could also be very important in understanding the diversity and additional characteristics of the Finnlakeviridae family.

1.5 Research questions and hypotheses

The first aim of this study was to characterize and document the diversity of Finnlakeviridae by comparing the genomes and life cycles of FLiP and the newly isolated FLiP-2 bacteriophage. A second aim was to confirm the unusual host dynamic characteristics of FLiP by comparing several host interaction behaviours with B330-P19 a different phage. The final aim was to characterize the newly isolated B330-P19 bacteriophage through electron microscopy and molecular analysis. We hypothesized that FLiP-2 would be almost identical in life cycle characteristics and genetic identity to FLiP due to their chloroform sensitivity and sequence similarity in the MCP gene mentioned earlier. Additionally, we hypothesized that the two FLiP phages would have different host dynamics in comparison with B330-P19. Finally, we also hypothesized that B330-P19 would be a tailed bacteriophage with no genetic identity to FLiP due to the lack of a lipid membrane.

2 MATERIALS AND METHODS

2.1 Bacterial and phage strains

In this work two previously characterized and two uncharacterized bacteriophages were used: PRD1 (Olsen et al. 1974), FLiP (Laanto et al. 2017b), FLiP-2 and B330-P19 (this study). FLiP was isolated from lake Jyväsjärvi (62°13.840’ N, 25°44.510’ E) in 2010 (Laanto et al. 2017b). FLiP-2 and B330-P19 were isolated from lake Jyväsjärvi (62°13.773’ N 25°44.273’ E) in 2021 from surface water. Additionally, several environmental *Flavobacterium. sp* strains isolated from around Finland were utilized (Table 1) to study phage host range. The bacterial strains were grown with either Shieh (Shieh 1980), LB (Bertani 1951), TYES (Holt et al. 1989) or High-tryptone cytophaga (HTC) (Smith 2019) medium.

To enumerate infective phage particles and study plaque morphologies, phage titration was performed using two different techniques: whole plate titration or drop titration both using the double layer agar method. Whole plate

titration was performed by mixing 100 µl of overnight grown bacteria and 100 µl of corresponding phage dilution in 3 ml Shieh or HTC soft agar (0.7% w/v) at 47 ˚C. The solution was immediately mixed and quickly poured onto a 1% agar plate made from the same medium. After 2 days of incubation in room temperature (RT) the plaques were counted to determine the plaque forming units per millilitre (PFU/ml) (i.e. titre) of the lysate. Drop titration was performed by adding only 100 µl of host bacteria into either Shieh, LB, TYES or HTC soft agar or low melt agarose (0.5% w/v) at 47 ˚C and poured onto a 1% agar plate of the same medium. Once the soft agar solidified, 10 µl drops of ten-fold phage dilutions were added on top of the plate and left to incubate in RT for 2 days after which phage titres could be counted and degree of lysis could be observed.

TABLE 1. List of *Flavobacterium* strains used and their origins. The known hosts of FLiP, FLiP-2 and B330-P19 are marked as "host". The host with which these phages were isolated from is marked as "main host".

Bacterial strain	**Isolation location**	**Citation**
Flavobacterium sp. B28	Lake Konnevesi	Laanto et al. 2011
Flavobacterium sp. B80	Lake Jyväsjärvi	Laanto et al. 2011
Flavobacterium sp. B105	River Vantaanjoki	Laanto et al. 2011
Flavobacterium sp. B121	River Tsarsjoki	Laanto et al. 2011
Flavobacterium sp. B127	Lake Kevojärvi	Laanto et al. 2011
Flavobacterium sp. B169	Lake Jyväsjärvi	Laanto et al. 2011
Flavobacterium sp. B171	Lake Valtimojärvi	Laanto et al. 2011
Flavobacterium sp. B174	River Kymijoki	Laanto et al. 2011
Flavobacterium sp. B176	Lake Leppävesi	Laanto et al. 2011
Flavobacterium sp. B178	Lake Äkässaivo	Laanto et al. 2011
Flavobacterium sp. B180	River Äyskoski	Laanto et al. 2011
Flavobacterium sp. B202	Hyytiälä	Unpublished
Flavobacterium sp. B205	Hyytiälä	Unpublished
Flavobacterium sp. B206	Lake Inari	Unpublished
Flavobacterium sp. B207	Lake Inari	Laanto et al. 2011
Flavobacterium sp. B208	Lake Inari	Unpublished
Flavobacterium sp. B209	Lake Inari	Laanto et al. 2011
Flavobacterium sp. B221	River Kymijoki	Unpublished
Flavobacterium sp. B222	River Kymijoki	Laanto et al. 2011
Flavobacterium sp. B223	River Kymijoki	Laanto et al. 2011
Flavobacterium sp. B224	River Kymijoki	Laanto et al. 2011
Flavobacterium johnsoniae UW101		Stanier 1947
UW10136 (HER1326)	Soil/water sample Madison, WI, USA	Richter & Pate 1988
Flavobacterium sp. B330 (**Main host**)	Lake Jyväsjärvi	Laanto et al. 2017b
Flavobacterium sp. B167 (**Host**)	Lake Jyväsjärvi	Laanto et al. 2011
Flavobacterium sp. B114 (**Host**)	River Kevojoki	Laanto et al. 2011

Phage lysate solutions were made by preparing a semi confluent Shieh agar plate (i.e. Shieh agar plate where around half of the bacterial lawn is lysed by phage) via the whole plate titration method as mentioned earlier with B330 as the host. Eight to ten ml of Shieh liquid medium was placed on the plate on a shaker

at 8 ˚C for 4 – 20 hours. The resulting lysate was collected and filtered through a 0.2 µm filter (Filtropur S, Germany) and stored at 8 ˚C.

2.2 Host range

To see if the phages had the ability to infect different hosts, the host range of FLiP, FLiP-2 and B330-P19 was determined by performing drop titration on Shieh agar plates with Shieh low melt agarose (see section 2.1) using several environmental *Flavobacterium* sp. hosts (Table 1). Serial dilutions of FLiP, FLiP-2 and B330-P19 stocks (with titers between 1-6x10^{10} PFU/ml) were made and 10 µl drops of each phage dilution were added onto the same plates to ensure direct comparisons. Each of the host/ phage combination was incubated at 8 ˚C, 18 ˚C or RT for two days before counting plaques. The hosts were suspected to be sensitive if the drops areas were either confluent (i.e. the area of the drop was completely lysed) or individual plaques could be seen. After initial screening, the potentially susceptible hosts were further confirmed to be susceptible by repeating the drop titration and performing whole plate titration on the potentially susceptible hosts. Finally, to test if different media would highlight differences in FLiP and FLiP-2 host ranges, drop titration was performed using LB, TYES, HTC and Shieh media, agar and soft agar.

2.3 Transmission electron microscopy (TEM)

Since the morphology of B330-P19 was unknown, it was studied with transmission electron microscopy (TEM). Formvar coated copper grids were glow discharged using a SC7620 Sputter Coater (Quorum Technologies) following manufacturer instructions. Subsequently B330-P19 lysate was added onto the grid for 60 seconds and dried by blotting. Immediately after, 2% phosphotungstic acid (PTA) was filtered through a 0.2 µm filter and added on top of the sample for 10 seconds, blotted and air dried for over a day. The samples were imaged using a JEOL JEM-1400HC TEM with 80 kV and RADIUS 2.1 (Build 20150, Emsis GmbH) software. The dimensions of capsids and tails were measured using the measuring tool from the software and the means and standard deviations were recorded.

2.4 Genome assembly and annotation

Illumina sequencing of the phage genomes was performed with purified B330-P19 DNA and FLiP-2 PCR amplified DNA before the start of this masters thesis by Novogene. The received Illumina paired-end short reads from FLiP-2 and B330-P19 were primarily analyzed using the Geneious software (v. 2.2.2022). First, short reads were trimmed using BBduk (v. 38.84) with default parameters. Outputted reads were assembled using Velvet (v. 1.2.10) with a k-mer length of 73 and using 1% of the reads. Assembled contigs were checked for completeness by overlapping the beginning of the sequence with the end. In the case of FLiP-2,

the overlapping end of the genome was deleted given that FLiPs genome is circular and nonredundant. Additionally, the short reads were mapped back onto the denovo assembled genome using the Geneious mapper to determine coverage and quality of assembly.

The assembled FLiP-2 genome was analyzed with a default parameter nucleotide BLAST search (Altschul et al. 1990) and the FLiP-2 short reads were aligned to the FLiP assembly downloaded from the NCBI database (Accession number: MF361639.1). The resulting alignment file was subjected to a single nucleotide polymorphism (SNP) analysis on the geneious software to identify and categorize the single nucleotide differences between the genomes. Based on alignment results the FLiP-2 assembled genome was reorganized according to the *Eco*RII site which defines the organization of FLiPs genome (Laanto et al. 2017b).

The assembled B330-P19 genome was also inputted into nucleotide BLAST search with search optimized for blastn, expected threshold of 0.001 and word size of 15. To determine the packaging mechanism of B330-P19, the coverage of read alignment on the reference assembled genome was analyzed using PhageTerm (v.1.0.12, Garneau et al. 2017)) on the Galaxy@Pasteur server (The Galaxy Community et al. 2022). The newly organized genome outputted by PhageTerm was searched for tRNAs and CRISPR motifs using the online softwares CRISPRCas finder (Couvin et al. 2018) and tRNA finder (Kinouchi and Kurokawa 2006).

Open Reading Frames (ORFs) were predicted from the newly organized genome outputted by PhageTerm using both Glimmer (Salzberg et al. 1998) and Genemark (Besemer and Borodovsky 2005). The predicted ORFs were manually checked from both software and included into the final annotation. If there was a disagreement on the size of the ORF, the longer one was included to the final annotation. The selected ORFs were translated to amino acid sequences (translation table 11, bacterial) which were further annotated using online softwares including the HMMER suite (v.3.1b2, Finn et al. 2011), Interpro (v.89.0, Paysan-Lafosse et al. 2023), BLASTp and PSI-BLAST. Within the HMMER suite, pHMMER was used against the UniprotKB (The UniProt Consortium et al. 2021) and PHROGs databases (v.4; Terzian et al. 2021) and HMMscan was used against the Pfam database (Mistry et al. 2021). The BLAST searches were against the non-redundant protein sequence (nr) database. The resulting annotations were curated, and the top functions were archived with corresponding E-values. In the final annotation the ORF was annotated with a function if there was a consensus on the annotation of the different softwares used and the e-value of at least one of them was below $1x10^{-5}$. If there was a conflict in the annotation, no annotation was given to the ORF.

2.5 Plaque size and identity analysis

Plaque sizes can be very informative on differences between bacteriophage life cycles. The plaques from whole plate titrations of FLiP, FLiP-2 and B330-P19 on

Shieh agar with B330 host were used for this analysis. The plates were imaged using a ChemiDoc™ MP Imaging System (Bio-Rad) with the colorimetric imaging option and increasing the contrast to a sufficient level. The resulting .tif files were further imported into Fiji (ImageJ, v.2.3.0, Schindelin et al. 2012) software and analyzed using the ViralPlaque macro (Cacciabue et al. 2019) a software that automatically detects plaques and retrieves pixel area of the plaque. Smaller plaques were not detected by this software and were manually encircled. The pixel diameters of the plaques were calculated from the pixel area assuming the plaques were perfect circles. The resulting pixel diameter of the plaques was converted to millimetres by using the 92 mm diameter petri dish as in the image as a reference. Phage plaques were only measured from one Shieh agar plate each.

To be certain that the morphologically different FLiP-2 plaques were from the same phage, 50 µl of lysate and three individual plaques of different sizes were sequenced using sanger sequencing method. Briefly, the three plaques and lysate were submitted to two PCR runs (30 cycles) using MCP and Replication initiation protein (RiP) primers (Appendix 1). The denaturation step was 95 ˚C for 30s, the annealing step was 62 ˚C for 30 sec and the elongation step was 72 ˚C 1 min. The reaction mixes were prepared with PCR grade water and DreamTaq DNA polymerase (Thermo Scientific, Lithuania). The resulting PCR products were purified using QIAquick PCR purification kit (Qiagen, Germany) according to the manufacturer's instructions. The sequencing reaction was done using BigDye Terminator v3.1 kit (Thermo scientific, Germany) with the same parameters as the revious PCR step. The sequencing reactions were run with capillary electrophoresis using an ABI Prisms 3130xl genetic analyzer (Applied Biosystems). The outputted data was automatically analyzed using Sequencing analysis software (v6.0, Thermo Fischer) and manually checked for errors using BioEdit sequence alignment editor (v 7.2.5, Hall. 1999).

2.6 Adsorption assay

The adsorption assay measures the kinetics of binding of phages to hosts. In total, 3 adsorption assays were performed where each phage (FLiP, FLiP-2 and B330-P19) was paired with B330 host. Each individual assay was performed with three biological replicates and a control with phage but no host.

The adsorption assay performed is a modified version of the Kropinski (2009) method. First, the host was grown overnight on a shaker at 120 rpm RT in HTC and diluted (with HTC) to an optical density of 0.1 at 595 nm (OD_{595}). The resulting medium was grown in a shaker at 120 rpm RT until OD_{595} 0.3-0.5, then diluted to a bacterial cell concentration of 2-5x10^8 CFU/ml (colony forming units per milliliter) and distributed to three different flasks. The bacterial cells were infected with MOI (multiplicity of infection) of approximately 0.0001 and aliquots were taken at the following timepoints (in minutes) post infection: 1, 2, 4, 6, 8, 10, 15, 30. The aliquots were diluted 1:20 in chilled HTC medium on ice to stop further adsorption. The diluted aliquots were centrifuged 8000 rpm for 3 mins in a MicroCL 17 tabletop centrifuge (Thermo) and 100 µl of the supernatant

was titrated on HTC agar plates using B330 as host to count the unadsorbed phage.

2.7 One step growth curve

Overnight grown B330 in Shieh medium was diluted, grown for approximately 5-6 hours to OD_{595} 0.5 in triplicate at 120 rpm, 21 ˚C and infected with each phage (FLiP, FLiP-2 and B330-P19) with MOI of approximately 0.075. The phages were allowed to adsorb to their hosts for 10 minutes after which the solution was centrifuged with a Sorvall RC 6+ centrifuge (Thermo scientific) using an F21-8x50y rotor (Thermo Scientific, USA) at 8000 rpm, 5 min, 21 ˚C. The supernatant containing the remaining unadsorbed phages was discarded and the pellet containing the hosts with the adsorbed phages was resuspended in the same volume of Shieh medium and placed back to the shaker. The resuspended bacteria-phage solution contained both a small proportion of unadsorbed phage that remained from the last step and bacteria that have been successfully infected in solution by one or more phages. Both the infected bacteria and free phages that form plaques on a bacterial lawn are collectively called infective centres. To determine the proportion and total amount of infected bacteria within the infective centres, the unadsorbed phage titre was determined and subtracted from the total infective centres. Unadsorbed phage was quantified immediately after resuspension by centrifuging an aliquot of the phage-bacteria solution at 8000 rpm, 5 min, 6 ˚C and determining the PFU/ml of the supernatant.

Next, the infection was allowed to continue until a point prior to the end of the phage life cycle as determined by prior tests: 150 min p.i. (post infection) for FLiP and FLiP-2 and 135 min p.i. for B330-P19. After this point, aliquots were taken from FLiP and FLiP-2 infections every 30 min for 180 min and titrated to observe when an increase in infectious centres would occur. In the case of B330-P19, aliquots were taken every 20 min for 210 min and titrated.

After counting the plaques, the burst size for each replicate was calculated i.e. the average amount of phages produced from one infected bacteria during one infection cycle. The burst size was calculated from the equation

$$\text{Burst} = \frac{N_f - \overline{N_b}}{\overline{N_b}} \quad (1)$$

where N_f was the highest infected bacteria titre reached and $\overline{N_b}$ was the mean of the infected bacteria titres prior to the large increase in titre (i.e. during the latent period).

Due to low sample size, differences in the burst sizes were tested with non-parametric analysis of variance Kruskal-Wallis test and further analyzed post hoc to identify which burst sizes were significantly different using Dunns test (Dunn 1964). The analysis was performed on the R software (v. 4.1.1, R Core Team. 2021) and the limit of statistical significance was 0.05.

2.8 Virion purification zymography and protein analysis

FLiP, FLiP-2 and B330-P19 were purified from phage lysates (with titres of approximately ~10^{10} PFU/ml) using PEG (Polyethylene glycol) precipitation and linear gradient centrifugation in 5-20% sucrose (in 20 mM KPO_4 buffer). First, high volumes of phage lysate (200-300 ml) were mixed into 10% PEG 6000 (Sigma-Aldrich, Germany) and 0.5 M NaCl and centrifuged with a Sorvall centrifuge and Fiberlite F12-6x500 LEX rotor (Thermo scientific, USA) at 8000 rpm, 30 min, 5 ˚C. The phage pellets were resuspended in 20 mM KPO_4 buffer (pH 7.2) and added on top of a 5-20% saccharose gradient. The saccharose gradients were ultracentrifuged with an Optima™ L-90K Ultracentrifuge (Beckman Coulter) using a SW41 rotor (Beckman) at 24 000 rpm, 14 ˚C, 1h (for FLiP and FLiP-2) or 35 minutes (for B330-P19). The light scattering bands were collected and ultracentrifuged with a 70.1 Ti rotor (Beckman) at 32 000 rpm, 5 ˚C, 3 h. The resulting pellet was resuspended in 20 mM KPO_4 and stored at -20 ˚C. The protein concentrations of the resulting purified phage aliquots were determined using Bradford concentration assay (Bradford 1976).

2.9 Protein analysis and zymography

The purified phage samples were prepared for protein analysis by Tricine SDS-PAGE by mixing them with 3x sample buffer (Appendix 2) and milliQ H_2O so that the total protein would be 10 and 30 µg. In addition, ultrapurified PRD1 and chicken egg lysozyme control samples were also mixed in sample buffer at the same concentrations. The resulting solutions were denatured by placing samples into boiling water for 5 minutes. The denatured phage particles with 10 µg protein were run on small modified 16% Tricine-SDS-PAGE gels and zymogels (Haider et al. 2012, Appendix 2) at RT, 100 V, 100 mA, 180 min. The 30 µg protein samples were run on a larger gel (Appendix 2) with a PageRuler Plus Prestained protein ladder (Thermo) standard at RT, 80 V, 20 mA, 20 h for a better separation of the individual proteins. The small gel was stained for 60 min with Coomassie blue and destained in 10% acetic acid for 30 minutes the first time and overnight the second time. The large gel was stained for 90 min with Coomasie blue and destained the same way as the smaller gel. Both gels were immediately imaged after destaining.

To determine which proteins belonging to the phages have peptidoglycan degradation activity, purified phages were run in a gel with peptidoglycan embedded inside (zymogel) and incubated at different temperatures. First, four small Tricine SDS-PAGE zymogels were prepared (Appendix 2) with two having *Escherichia coli* and the other two having *Flavobacterium sp.* B330 peptidoglycan. As previously, the 10 µg protein samples were run on these zymogels. One of each zymogel types were run at RT, 100 V, 100 mA, 180 min and the other two were run at 6 to 9 ˚ C (cold treatment) with same parameters for 260 min. After the run, the four gels were inoculated in renaturation buffer (25 mM KPO_4 0.1% Triton X-100 (Sigma, USA), pH 7.2) on a Roto-shake genie (Scientific Industries)

for 30-70 hours at corresponding temperatures with a change of renaturation buffer after the first 12-20 hours. The gels were stained with 0.1% methylene blue in 0.01% KOH in a shaker for 60 min followed by first destaining on the shaker with milliQ water for 30 min followed by another destaining for 30 min. The gels were further destained overnight if it was deemed necessary in order to get sufficient contrast between the areas where the peptidoglycan was degraded. The gels were imaged immediately after destaining.

3 RESULTS

3.1 Host ranges between FLiP and FLiP-2 differ slightly

Initial screening of phage host range (in June 2022) revealed that out of 26 strains, only B330, B167 and B114 had visible plaques by all three phages as expected. B330-P19 infected three other strains that FLiP and FLiP-2 did not (Table 2). Suprizingly, FLiP was observed producing plaques on B80 while FLiP-2 did not (Table 2). The observed host range was transient however and the abilities of FLiP to produce plaques on B80 and B330-P19 on B167 and B114 were lost after replicating the experiment after several months (October 2022).

TABLE 2. Host range results showing *Flavobacterium* sp. that were susceptible to at least one of the three bacteriophages tested. The titres on the susceptible hosts were also recorded.

	FLiP	FLiP-2	B330-P19
B28			**X** ($9x10^6$ PFU/ml)
B80	**X** ($1.04x10^8$ PFU/ml)		
B205			**X** (ND)
B169			**X** ($1.36x10^9$ PFU/ml)
B114	**X** (ND)	**X** (ND)	**X** (ND)
B167	**X** (ND)	**X** (ND)	**X** (ND)
B330	**X** ($4x10^{10}$ PFU/ml)	**X** ($5.2x10^{10}$ PFU/ml)	**X** ($1.43x10^{10}$ PFU/ml)

X = susceptible ND = Titre on host not determined

The second set of host range experiments was performed using Shieh, LB, TYES and HTC media to find if different conditions magnified the possible different host range of FLiP and FLiP-2. As mentioned previously, this was performed using the *Flavobacterium* sp. B330, B167, B114, B80 and B169. During these experiments (January 2023), the most striking result was the inability of B330-P19 to produce plaques in B114, one of its previously determined hosts (Figure 3B). Further, although both FLiP and FLiP-2 produced plaques on Shieh, TYES and HTC plates normally, titres dropped several orders of magnitude when titrations were performed with LB medium. However, with B114 and B330 hosts plated with LB, one phage was affected more than the other. Specifically, with B330, FLiP-2 produced plaques at high dilutions while FLiP produced plaques albeit very turbid ones and not until such a large dilution as FLiP-2 (Figure 3A). When both phages infected B114, the effect was almost reversed with FLiP producing plaques at high dilutions while FLiP-2 produced no plaques at all and only inhibited bacterial growth until -1 dilution (Figure 3B).

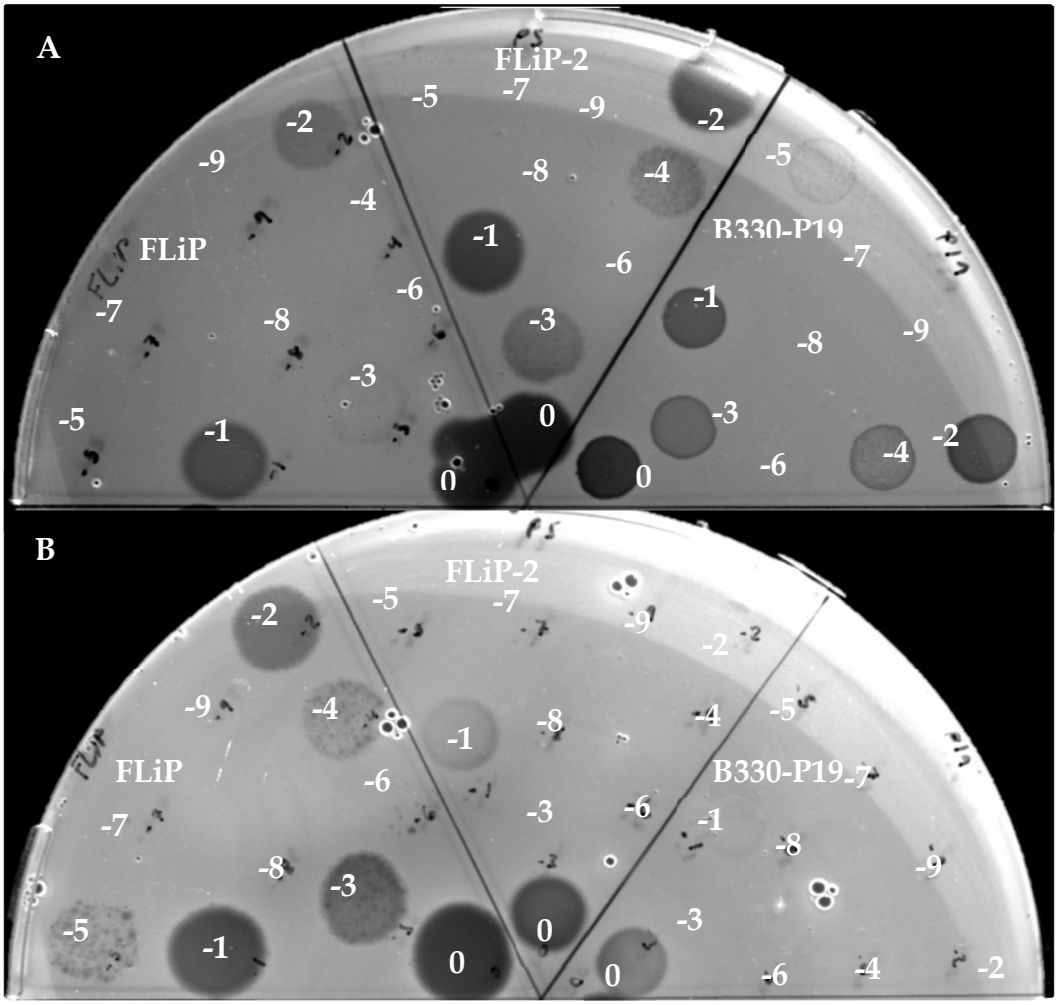

Figure 3. 140 mm petri dish with *Flavobacterium sp.* B330 (A) and B114 (B) grown in LB and plated on LB agar with LB soft. The plate was divided into three parts with the left containing diluted drops of FLiP, the center diluted drops of FLiP-2 and the right diluted drops of B330-P19. The dilutions of each phage was from 0 (i.e. no dilution) to -9 (i.e. 10^{-9} dilution). The stocks from which the dilutions were made, had titres of ~10^{10} PFU/ml according to B330 titration on HTC.

3.2 B330-P19 is a tailed bacteriophage of its own lineage

Transmission electron microscopy of B330-P19 revealed particles with a mean icosahedral capsid facet to facet width of 113 nm (SD 6, n = 14) attached to a rigid (i.e. not flexible) tail with a mean length 170 nm (SD 8, n = 14) and without tail fibres (Figure 4A-C). Additionally, some capsids were attached to a contracted tail with a mean length of 125 nm (SD 8, n = 10) (Figure 4B-C). Closer inspection of the contracted tail reveals small structures protruding horizontally from the baseplate on both sides that were not present on the longer counterpart.

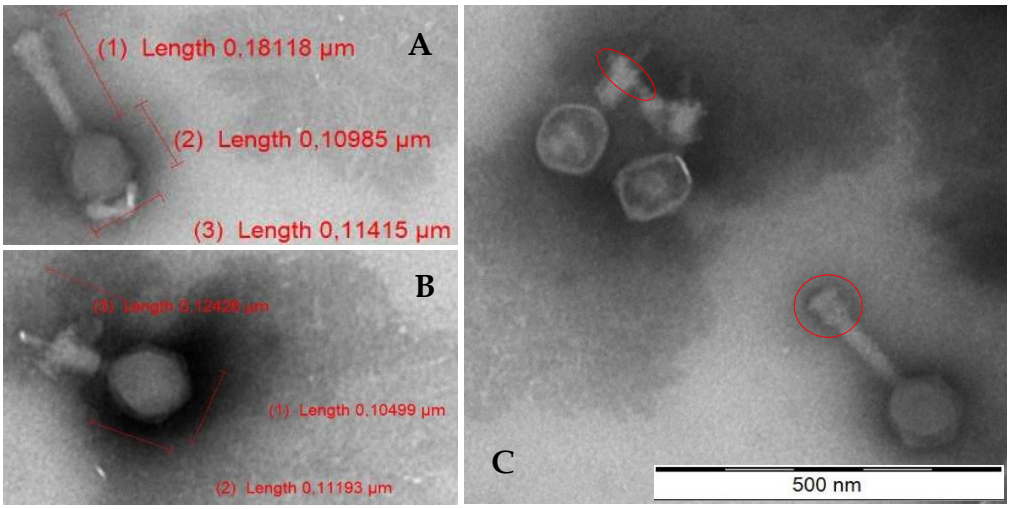

Figure 4. Transmission Electron Microscopy (TEM) images of B330-P19 stained with 2% PTA. A) a single B330-P19 virion with a head and tail. B) Close up of a B330-P19 virion with a contracted tail. C) Different B330-P19 morphologies on the same screen with a scale bar and the baseplates circled in red.

De-novo assembly of B330-P19 reads outputted a single contig 167 814 bp long with a mean coverage of just under 8000. PhageTerm determined that B330-P19 had circularly permuted repeats and a Head-full Pac packaging mechanism. In total 195 ORFs were predicted on both DNA strands of which 20% were annotated with a function. Examples of a few key annotated proteins were a terminase, tail sheath and major capsid protein (Appendix 3). Annotation software found no tRNAs or CRISPR-Cas systems. BLASTn found no closely related phages to B330-P19 although a significant hit from base pairs 66 730 – 66 910 on B330-P19 were 75-73% homologous in cellulophaga phages phi17:2 and phi4:1 respectively.

3.3 FLiP and FLiP-2 have similar genomes

De novo assembly of FLiP-2 revealed 9176 nucleotide long, circular genome with a mean coverage of just under 174 000. Aligned with my hypothesis, FLiP and FLiP-2 were shown to be highly related with an average nucleotide identity of 96.64%. FLiP-2 differed at 303 nucleotide positions with FLiP, having 299 SNPs, 3 insertions and one deletion.

Most of the identified SNPs in protein coding sequences were synonymous (i.e. no amino acid change). However, 41 amino acid differences were predicted based on the few nonsynonymous SNPs (i.e. amino acid change, Table 3). Furthermore, there were no major differences in amino acid lengths detected between FLiP and FLiP-2. Amino acid differences did seem to concentrate to the beginning of the genome where there was a relatively high amino acid change / protein length ratio. In addition, although several of the differences were found in hypothetical proteins with no known functions, a few amino acid differences were in proteins with hypothesized functions. The hypothetical spike protein (ORF 13), likely involved in phage attachment to the host, had four neutral amino acid differences (i.e. amino acid changed to one of the same polarity) and one amino acid class change (i.e. amino acid changed to one of different charge or polarity). Moreover, two neutral amino acid changes were present in GP 7 while one neutral and one class changes were present in GP 14. Both of these proteins are thought to have muralytic activity (i.e. degrade peptidoglycan). These proteins were relevant because the differences in their hypothetical functions could be tested with an adsorption assay and zymography. Additional changes were observed in ORF 4, GP 8 and ORF 15.

TABLE 3. Differences in the putative amino acid sequences between FLiP and FLiP-2 and their lengths and annotations. Highlighted proteins may have phenotypic effects on viral life cycle that can be tested.

ORF	Protein length (in AA)	Annotation	AA changes	Additional changes
ORF 1	97		1 N	
ORF 2	81		1 N, 4 C	
ORF 3	101		5 N, 4 C	
ORF 4	140-141	Helix-turn helix motif (Laanto et al. 2017b)	5 N, 1 C	Start codon loss in FLiP-2
ORF 5	70			
ORF 6	73		1 N, 1 C	
GP 7	85	**Putative lytic protein** (Mäkelä 2019)	2 N	
GP 8	312	Major capsid protein (Laanto et al. 2017b)	4 N, 1 C	
GP 9	124			
ORF 10	159		1 N	
GP 11	159			
ORF 12	149	Penton base (Unpublished data)		
ORF 13	337	**Hypothetical spike** (Unpublished data)	4 N, 1 C	
GP 14	222	**Lytic transglycosylase** (Laanto et al. 2017b)	1 N, 1 C	
ORF 15	448	Replication initiation protein (Laanto et al. 2017b)	2 N	
ORF16	82		1 C	

AA = amino acid N = neutral change C = class change

3.4 FLiP and FLiP-2 have different plaque morphologies

Plaque morphology is an important phenotype of bacteriophage biology which highlights differences between phages and is especially important for titre calculations. FLiP plaques were characterized as having fuzzy edges (Figure 5A) and a mean diameter of 0.88 mm and a large variation in sizes (Figure 6). When FLiP-2 was first isolated, it had a similar plaque morphology as FLiP, yet at the start of this study they had become different. Sanger sequencing of PCR products from the major capsid protein and replication initiation protein revealed that these plaques, although different in morphology, were indeed FLiP-2 (see section 3.3). FLiP-2 plaques were characterized as having similarly fuzzy edges (Figure 5B) and noticeably smaller plaques with a mean diameter of 0.54 mm yet also high variety in sizes (Figure 6). This plaque morphology was observed even when the original plaque isolate of FLiP-2 was titrated with revived B330 stock used from the time of the original isolation. Both FLiP and FLiP-2 plaques were noticeably different from those of B330-P19 which had a sharp edge (Figure 5C) and relatively more homogenous plaque size with a mean size of 0.51 mm (Figure 6). The differences in plaque morphologies were similarly observed with both B167 and B114 hosts, although the differences were in some cases more extreme (Appendix 4). Oddly however, B330-P19 was observed to not infect B167 or B114 after the experiments resumed in the winter season (January 2023).

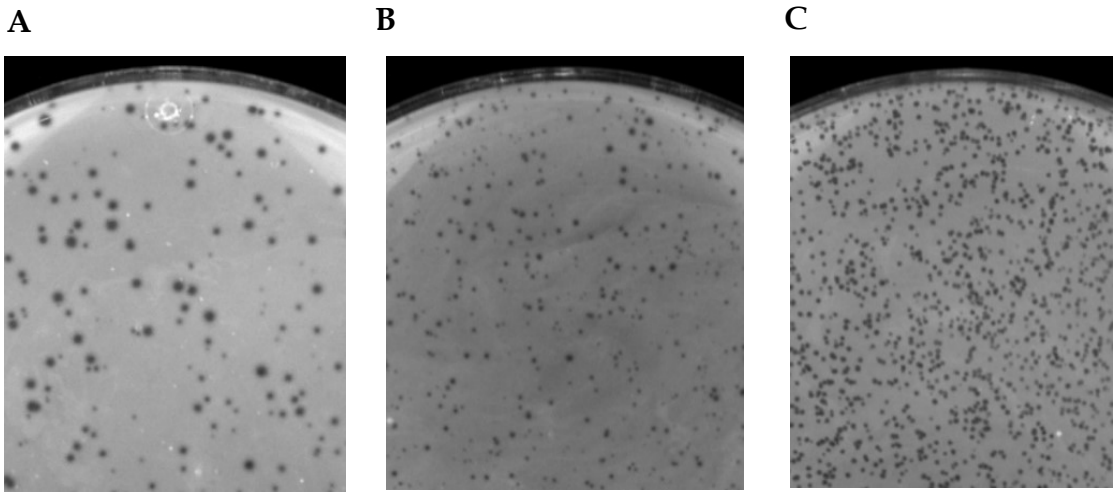

Figure 5. Images of plaques from different phages on 92 mm petri dishes with Shieh agar and B330 host. A = FLiP, B = FLiP-2 and C = B330-P19.

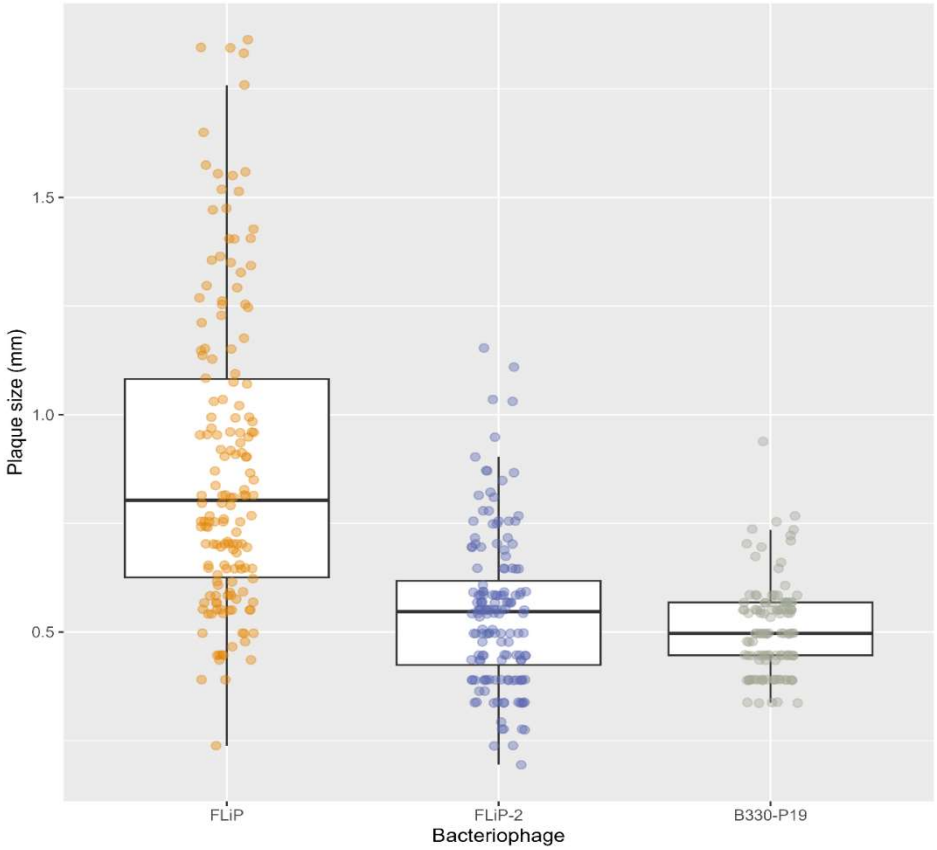

Figure 6. Boxplot of the distribution of plaque diameters (mm) of different bacteriophages as determined by ImageJ pixel measurements in relation to petri-dish size. Each measurement was taken from plaques on three Shieh agar plates with B330 host. The number of measured plaques for FLiP, FLiP-2 and B330-P19 were 158, 152 and 119 respectively.

3.5 Phage adsorption was not consistent

Adsorption assays are standard techniques measuring the kinetics of bacteriophage attachment and hence could reveal differences in attachment efficiencies between FLiP, FLiP-2 and B330-P19 on their host bacteria. In this case, these assays revealed that none of the bacteriophages consistently adsorbed to B330 host throughout the assayed time period. After one minute, only a small fraction of FLiP, FLiP-2 and B330-P19 adsorbed to cells and the fraction did not increase consistently and sometimes even decreased.

3.6 FLiP and FLiP-2 have a different life cycle in comparison with B330-P19

The one step growth curve provides information on the timing of different periods during a single infectious cycle of a virus and can provide an estimate for how many phages are produced per infected cell. In the case of FLiP, after attempting to remove unadsorbed phage by decanting the supernatant

immediately after pelleting (see methods) a total of $2x10^6$ PFU/ml were left unadsorbed. At 152 min p.i. the total amount of infective centers was on average $6x10^6$ PFU/ml meaning that $4x10^6$ PFU/ml of the infective centres are caused by infected bacterial hosts and 33% of the infective centers correspond to unadsorbed phages. Titers seemed to start to increase between 150-180 min p.i. but previous tests have shown that the increase started between 180-200 min p.i. (Appendix 5) and that there is a large variation in titres before that. The point where the titers start increasing marks the end of the latent period and start of the burst period. Here, the titres kept increasing until it reached a peak of $4.22x10^7$ PFU/ml at the end of the sampling period and did not clearly plateau (Figure 7A). Just prior to the last sampling period there was also a small decrease in titer relative to the last time point making a small dip in the graph. Using the equation 1 with each replicate, it was established that the median burst size of FLiP in these conditions was 4.58.

As expected, results from the one-step growth curve with FLiP-2 were similar to those of FLiP. After pelleting, the titres of unadsorbed phage virions were determined to be $6x10^6$ PFU/ml. At 150 min p.i. the infective center titres were $1.01x10^7$ PFU/ml meaning that $4x10^6$ PFU/ml infected bacteria were present and that the unadsorbed phages corresponded to about 60% of the total infective centers. The latent period lasted until 180-210 min p.i. after which titers started to increase and reached a peak of $3.5x10^7$ PFU/ml at the end of the sampling period (Figure 7B). Again, using equation 1 on each replicate, it was determined that the median burst size of FLiP-2 was 2.63. The small difference in burst size between FLiP and FLiP-2 was not statistically significant.

The one-step growth curve of B330-P19 with B330 was different as expected. After removing the unadsorbed phage after pelleting, $3x10^5$ PFU/ml phage particles were left unadsorbed. However, the total amount of infective centres at 135 min p.i. was $1.9x10^7$ PFU/ml on average. Subtracting the unadsorbed phage from the infective centres reveals the number of plaques which were formed from infected hosts. Given that the unadsorbed phage formed only 1.6% of the infective centers, the number of infected hosts was $1.8x10^7$ PFU/ml. The phage titres started increasing between 215 and 235 min p.i. From the start of the burst period, the titers kept climbing until the end of the sampling period (Figure 7C). At peak titer, the B330-P19 rose to a titre of $6.7x10^8$ PFU/ml on average but was not observed to plateau during the sampling period, even though titres increased over

a period of 70 minutes. This time the median burst size from the three replicates was determined to be 27.73.

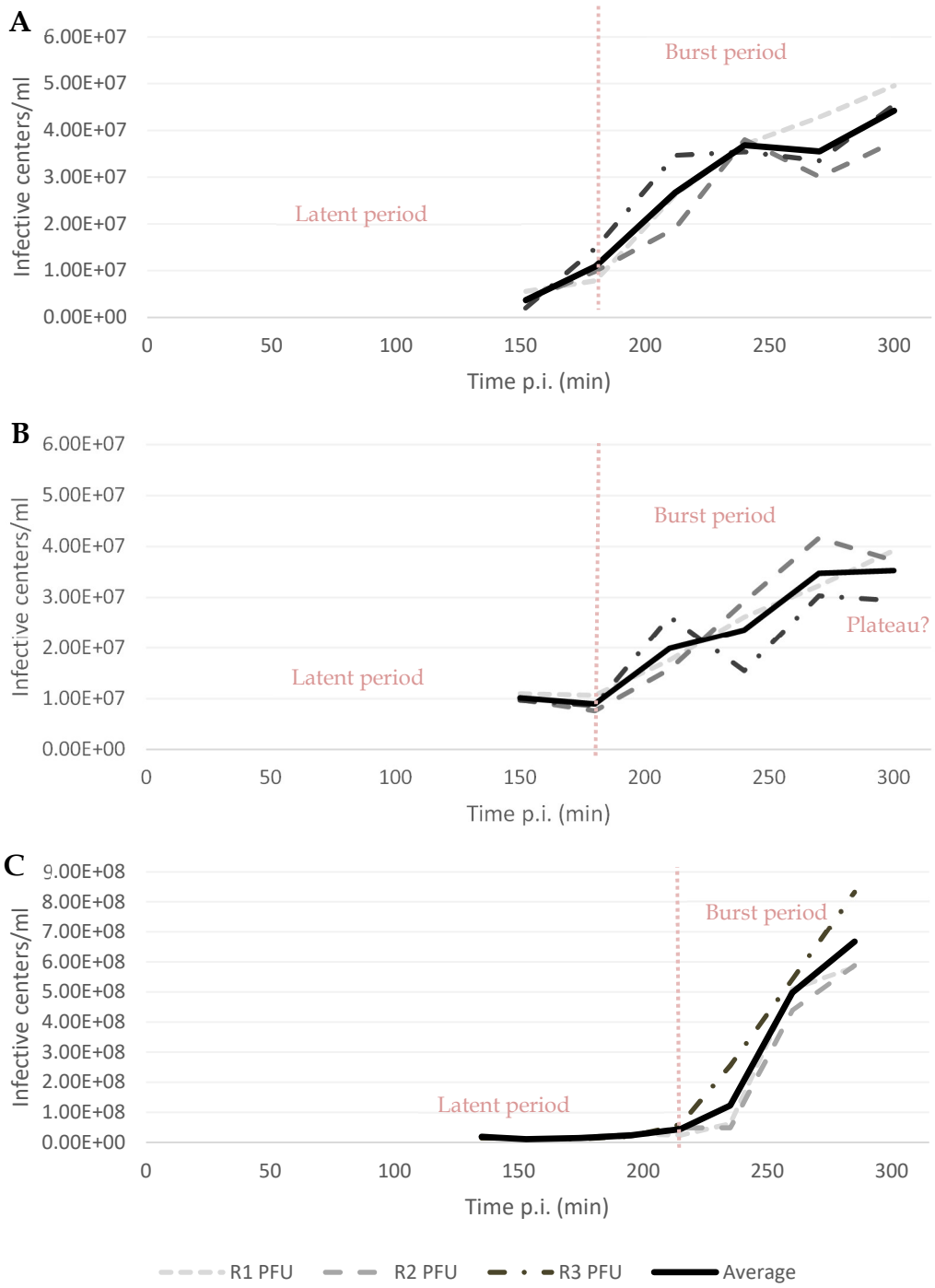

Figure 7. One step growth curves of A) FLiP, B) FLiP-2 and C) B330-P19 with B330 host showing the timing and magnitude of titre increase. The X-axis shows the time in minutes post infection and the Y-axis represents the increase in bacteriophage titers measured in Infective centers per ml. The bacterial culture was infected at OD 0.5 with MOI 0.075 and infections were performed in triplicate. The graphs are divided into the latent period and burst period.

3.7 The two FLiP strains structural proteins were similar

To get a brief overview of the structural proteins of the two FLiP strains and B330-P19, virions were first purified with a 5-20% linear saccharose gradient providing a protein yield of 2.5, 2.4 and 1 µg/µl for FLiP, FLiP-2 and B330-P19 respectively. These purified proteins were run on a large tricine SDS-PAGE gel to separate the proteins by size. Observing the lanes with the two FLiP strains it is quite apparent that the protein profiles of both phages look almost identical (Figure 8). Interestingly when looking at the annotated protein bands on the FLiP lane, one sees that in the areas where there should be one structural protein, there are two bands (GP 14 and GP 11). Additionally, in the area where GP 7 and GP 9 are, there is only one large band. Compared to the scarce number of proteins seen with the two FLiP strains B330-P19 seems to have a larger number of them (Figure 8).

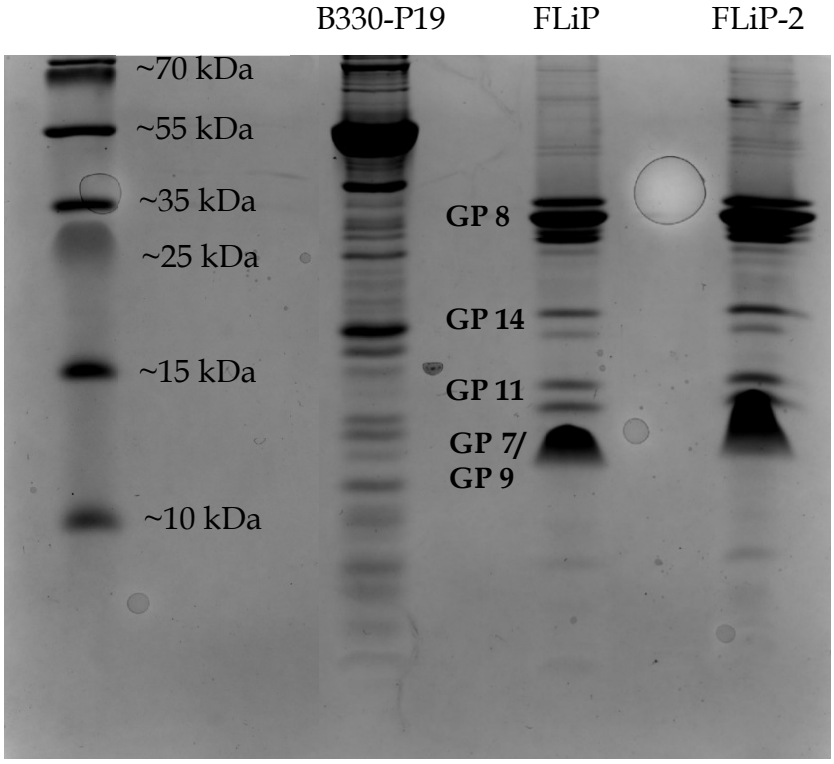

Figure 8. Large Tricine SDS-PAGE gel with 30 µg of 5-20% linear saccharose gradient purified B330-P19, FLiP and FLiP-2 in different wells with proteins separated by molecular weight. The FLiP well proteins are annotated with the structural proteins that were defined prior (Laanto et al. 2017). The first well corresponded to the PageRuler Plus Prestained ladder.

3.8 FLiP and FLiP-2 lytic enzymes have different activities

To observe whether peptidoglycan hydrolases were present on any structural protein of B330-P19 or had any difference in activity between FLiP and FLiP-2, purified virions were assayed with zymogels using *E. coli* and B330 peptidoglycan. For B330-P19, no unstained bands were visible on any of the zymogels. For the two FLiP strains, different unstained bands could be observed in the *E. coli* and B330 zymogels incubated in renaturation buffer at RT or 6 to 9 ˚C (cold treatment). First, the *E. coli* and B330 zymogels incubated at RT produced one or possibly two bands almost on top of each other for FLiP and FLiP-2. These bands were located at around the same height as that of lysozyme between 15 and 10 kDa (Figure 9A and C). The same bands were observed at similar intensities in the E. coli and B330 zymogels incubated in the cold (Figure 9B and D). An additional band was observed in the cold incubated *E.coli* zymogel but not the cold incubated B330 zymogel for both FLiP and FLiP-2 just below 25 kDa. Surprisingly, even though both FLiP and FLiP-2 produced a band at around 25 kDa, the band produced by FLiP was brighter in comparison. Another observation of note is that the bands corresponding to GP 7 have an interesting wavy shape which is not observed in any other band. The wavy band is also observed in tricine SDS-PAGE gel without peptidoglycan and stained with coomasie blue.

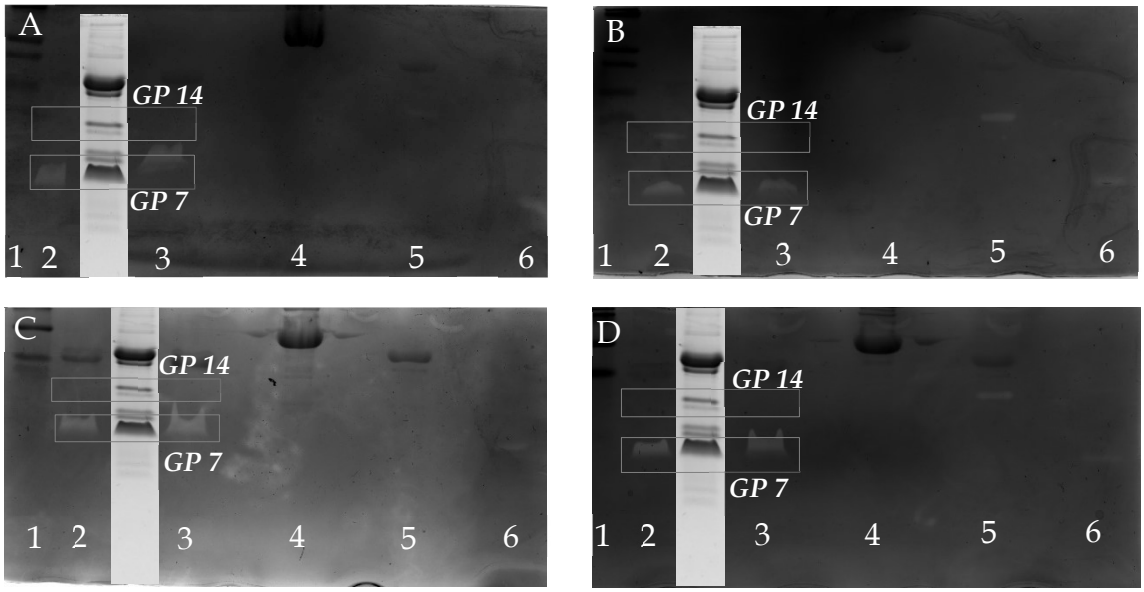

Figure 9. A) and B) Zymograms where E. coli peptidoglycan was used with RT and cold treatment respectively. C) and D) Zymograms where B330 peptidoglycan was used with RT and cold treatment respectively. Numbered wells were loaded with corresponding samples: 1. Prestained protein ladder. 2. Purified FLiP. 3. Purified FLiP-2. 4. Purified B330-P19. 5. Purified PRD1. 6. Purified checken egg Lysozyme. All wells were loaded with 10 µg protein as determined by Bradford assay. In between wells 2 and 3, a run of 10 µg of the same FLiP sample on a small tricine SDS-PAGE gel was added with annotated structural proteins as a reference.

4 DISCUSSION

FLiP is an unusual phage isolate representing a recently discovered branch of virus evolution having an ssDNA genome, a lipid membrane and more in common with varidnaviria dsDNA phages than other ssDNA phages. Previous work has shown that it has an unusual life cycle where it reproduces effectively on agar plates yet not in liquid culture. Although FLiP is the only representative of the species *Finnlakevirus FLiP* in the *Finnlakeviridae* family, two new phages infecting the same three hosts as FLiP have been isolated. The new isolates were called B330-P19 and FLiP-2. This work had three primary aims: To understand the genetic and phenotypic diversity of *Finnlakviridae* phages, to confirm the unusual phage-host interactions of FLiP by comparing it with a control phage and to characterize a newly isolated bacteriophage. It was hypothesized that FLiP and FLiP-2 closely related and have similar phage-host interaction dynamics while B330-P19 would be different. Additionally, it was hypothesized that B330-P19 would be a typical tailed phage.

4.1 *Finnlakevirus FLiP* genetic diversity

As was hypothesized, FLiP and FLiP-2 were highly related with a 96.64% nucleotide identity between each other indicating that FLiP-2 is a strain of the *Finnlakevirus FLiP* species according to the ICTV taxonomy guidelines (Adriaenssens and Brister 2017). This interpretation is further supported by the similarity in the protein size profiles of the two phages. From an evolutionary biology point of view, that FLiP has so many differences from FLiP-2 also suggests either that the former has been replaced by the latter in the natural population or that at least two subpopulations of *Finnlakevirus FLiP* may be coexisting in the area. The first scenario is perhaps best explained by the evolutionary arms race occurring between bacteria and phage. Indeed, several artificial and semi natural systems have shown that bacteriophages rapidly adapt in response to bacterial phage resistance mechanisms (Gómez and Buckling 2011; Laanto et al. 2017a; Kortright et al. 2022). In this scenario, FLiP started to accumulate selective mutations, which would allow for escape from various resistance mechanisms that bacteria are known to have (see Rostøl and Marraffini 2019; Wang et al. 2023), eventually leading to the extinction of FLiP and giving rise to FLiP-2. It is also of course possible that both FLiP and FLiP-2 exist at the same time in which case their differences may be mainly reflective of their different niches (i.e. host preference). This possibility is also likely since it has been extensively shown in animal viruses and phages that upon several passages on a new host, mutations accumulate as selection favours phenotypes that are better adapted to the new host (Xu et al. 2014).

The detection of a second *Finnlakevirus FLiP* isolate increases the known diversity of this species although a single additional isolation is likely not

representative of its true diversity in its natural habitat. However, the fact that it has been eleven years since the last isolation argues that *Finnlakevirus FLiP* has an established presence in the environment. The rare isolation of *Finnlakeviridae* phages is not unexpected given that very little is known about the ecology of these elusive bacteriophages and their hosts. *Finnlakevirus FLiP* virions may be more abundant at different depths of the lake where their hosts are more abundant rather than surface waters as has been demonstrated to be the case for phage communities in aquatic environments (Goddard et al. 2005; Winter et al. 2009; Goldsmith et al. 2015). That *Flavobacterium* sp. relies on a solid surface requiring, gliding motility system for locomotion (section 1.3) may be a strong indication that FLiPs host is not primarily found in the water column and may be more concentrated of surfaces. If a surface is required, *Finnlakevirus FLiPs* natural host may have a niche in the sediment at the bottom of the lake (e.g. He et al. 2017), on the surfaces of plants (e.g. Parena et al. 2022) or on mucosal surface of fish (e.g. Barr et al. 2013). Even though FLiP lacks immunoglobulin-like domains necessary for mucosal surface binding like several other mucous-associated phages (Barr et al. 2013) there is some evidence supporting the idea of FLiP might associate with fish. Specifically, an annotated metagenome assembled genome (MAG) from a sample of red snapper tissue had homology with several of FLiPs proteins (Tisza et al. 2020; GenBank: MH617761.1) lending support to the idea that FLiP may accumulate on fish tissue. Alternatively, it is also not impossible that *Finnlakevirus FLiP* and its host have a primary niche in a nearby lake which feeds into lake Jyväsjärvi or even nearby terrestrial soil and the samples obtained are only remnant virions washed into the lake. Indeed, viruses can be abundant in niches where their hosts do not primarily live like plant viruses found abundantly in human guts and oropharynx which presumably are ingested with plant matter (Aguado-García et al. 2020). All the previously mentioned alternative FLiP niches may explain why FLiP phages are not as present in sampled water columns.

To understand the true diversity, ecology and evolutionary biology of *Finnlakeviridae* phages, extensive bacteriophage isolation and metagenomic sampling of lake Jyväsjärvi and the surrounding lakes at different depths and from different surfaces would need to be undertaken. Additionally, this should be accompanied with bacteriophage isolation efforts to find out if the genotypic differences between the different phages may have some phenotypic effects. Indeed, such an undertaking may provide further support to the idea that this unusual phage type is widespread as discussed in section 1.4. On a broader point of view to understand the global diversity of these exotic phages, different surfaces near or in aquatic environments should be sampled without the use of lipid degrading agents like chloroform which is routinely used for bacteriophage isolation as mentioned in section 1.2.2. Taken together, the second isolation of *Finnlakevirus FLiP* after eleven years suggests that this species has an established presence in lake Jyväsjärvi, the surrounding environment or both and may have an important ecological role.

4.2 FLiP and FLiP-2 phenotypic differences

The stark differences in plaque morphology and size between FLiP and FLiP-2 on B330 and B114 hosts are a clear sign that functional differences between the two strains are present despite highly similar genomes. This interpretation of functional differences is further supported by differences in host range and the large differences in plaque visibility caused by culturing with LB medium. Although these differences could be caused by the putative amino acid differences highlighted earlier, other options are also possible. Indeed, key changes in non-coding regions can have effects on putative conserved ssDNA secondary structures (Muhire et al. 2014), transcription factor binding sites and/or interactions with ribosomes, altering gene expression and translation (Kershner et al. 2016; Baranovskaya et al. 2019; Rojano-Nisimura et al. 2020). The phenotypic differences may not even need to be caused by nucleotide polymorphisms and could be due to more subtle differences like epigenetics (Hattman and Fukusawa 1963; Seong et al. 2022). As such, to establish causality of the phenotypic changes, recombination experiments with both FLiP strains or targeted mutations with CRISPR-CAS (Jinek et al. 2012) could be implemented to FLiP. The mutated phages could then be tested to see if host range and plaque morphology remains similar. Additionally, more specific assays targeting inherent phage capabilities like adsorption or burst size could be performed. These are important questions to follow up on as they can lead to new discoveries in the uncharacterized molecular biology of lipid containing ssDNA phages.

Interestingly, although the discussed contrast in plaque morphology and host range was used to infer phenotypic difference between FLiP and FLiP-2, both the host range and plaque morphology did not remain constant for either phage respectively. At least the change in plaque morphology is unlikely to be caused by mutations in phage or bacteria given that the different plaque morphology of FLiP-2 was observed even when titration was performed with the original FLiP-2 plaque and B330 stock used in 2021 for its isolation. It is also unlikely to be caused by cross-contamination as confirmed by sanger sequencing of individual plaques and whole lysates. As such, a more likely explanation is that some cryptic environmental factor has changed. The interpretation that the environment plays a key role is also supported by the observation that previously, both FLiP and B330-P19 have been observed to transiently change their host ranges (Mäkelä 2019; unpublished data). This could be caused by minor differences in media compositions due to ingredients that have different molar compositions from batch to batch like tryptone, which can be produced from non-standardized ingredients (e.g De Spiegeleer et al. 2004; Turki et al. 2009). This change in phenotype could be interesting to follow up given that it can provide answers to fundamental questions about the molecular biology of the host and *Finnlakevirus FLiP*. For follow up experiments, it would be important to replicate the original plaque morphology of FLiP-2 and host range of FLiP to tease out some mechanisms of what causes these differences.

The host range experiments in different conditions brought up some interesting discussion points as well. That host range results can change so

dramatically due to changes in medium is perhaps not that surprizing given that bacteria can rapidly change phenotypic characteristics in different conditions (De Spiegeleer et al. 2004; Turki et al. 2009) which can affect phage infections in various ways (Inomata et al. 2012; Qin et al. 2017). However, this has large implications given that the primary analysis done on bacteriophage isolates are plaque assays. Specifically, that FLiP-2 drop titrations only inhibited B114 growth on LB until 10^{-1} dilution drop would be considered as evidence of no infection. If such drop titrations had been performed only with LB, it would have never been known that FLiP-2 can infect B114. The broader implication of such a result is that this may also occur for other bacteria – phage interactions in which case perhaps some phages are not identified during screening attempts. During a time when antibiotic resistant bacteria are becoming more abundant and more efforts are being placed in phage isolation for therapy (Uchiyama et al. 2008; Lin et al. 2017), perhaps to maximize the number of bacteriophages found, one could try discovery using at least two different media. Such a process may also be important in elucidating further diversity of bacteriophages in nature.

FLiP and FLiP-2 had a similar life cycle with the one-step growth curve experiments although a few key differences were also noticed. The latent period and the amount of unadsorbed phage particles was highly similar between FLiP and FLiP-2 which was to be expected given the close relatedness. However, both bacteriophages were shown to be different in their burst sizes, with FLiP having a larger one than FLiP-2 (4.58 and 2.63 respectively). Although this could be a possible explanation for the difference in plaque size, the burst size difference was non-significant. There is however a large caveat that complicates of this interpretation: the lack of a plateau phase in the one-step growth curve during which the titre increase stops as a signal that all infected cells in the beginning have burst (Hyman and Abedon 2009). Although in the case of FLiP-2 the last two sampling points were very close to each other, at least a third sampling point would be needed to confirm that the titers had indeed plateaued. Hence, the calculated burst sizes are not strictly speaking correct and could be higher. Additionally, the burst size of FLiP is a little bit larger- and the overall shape of the one-step growth curve is different here than that reported by Mäkelä (2019). In that study performed with HTC media, it was reported that the burst size was about 1.5 and that titers had a sharp drop after about 150 min p.i. and leading up to a second rise later. Although the different culture media used and even the different OD_{595} at which the bacteria were infected in this study could explain the difference in the burst sizes (e.g. Inomata et al. 2012; Qin et al. 2017), it is harder to explain the absence of the sharp titre drop observed originally. Due to these caveats, it cannot be confidently said whether FLiP and FLiP-2 differ in their burst sizes and the experiments should be repeated.

The adsorption assay performed with both FLiP and FLiP-2 returned some unexpected results since they did not attach effectively to B330, their main host. This runs in contrary to the previous experiments (Marjakangas 2014; Mäkelä 2019) where FLiP managed to attach effectively to B330. Previously, it was only with B167 and B114 where FLiP did not attach very effectively (Mäkelä 2019). It

is hard to find a more attractive explanation other than environmental changes discussed earlier given that this assay was performed in the same way as described by Mäkelä (2019). However, large fraction of unadsorbed phage after pellet resuspension in the one step growth curves of FLiP and FLiP-2 provide an interesting alternative explanation. When the infected cells are centrifuged, only the phages attached to the bacteria should be in the pellet and most of the unattached phages in the supernatant should have been removed. Hence, the large percent of unadsorbed phages after resuspension would be those that were attached to the host but got unattached during resuspension. If this is the case, then perhaps *Finnlakevirus FLiP* detaches easily from its host when it is in its reversible attachment phase (see section 1.1). Although models of reversible and irreversible attachment were mostly established with tailed bacteriophages (Storms and Sauvageau 2015), phiX174 (a non-tailed, ssDNA phage) has been proposed to attach following the same model (Roznowski et al. 2019). Similarly, phage PRD1 (same realm as FLiP) is hypothesized to reversibly attach and roll on the surface of the bacteria cell until it reaches a final destination where it injects its DNA after irreversible binding (Strömsten et al. 2003; Peralta et al. 2013). This could possibly explain the contrasting adsorption assay results obtained with those of previous experiments since a large part of adsorption assay involves shaking the medium to ensure homogeneity. This is normally done by hand and is not standardized which could imply that the shaking done here may have been too vigorous and detached most phages. It would not be hard to imagine that vigorous shaking could detach the weakly bound virions. As such, perhaps further adsorption assays could be performed without shaking to see if this would improve adsorption rate. Furthermore, it would be important to perform this experiment given that several nonsynonymous differences were found on the putative spike protein between both FLiP strains. Generally, it is thought that the spike proteins are the key host recognition proteins like in the case for phages PRD1 and phiX174 (Kawaura et al. 2000; Strömsten et al. 2003; Peralta et al. 2013; Roznowski et al. 2019). If there were a measurable difference in adsorption between the two FLiP strains, it would make it likely to be due to one of those key nonsynonymous mutations.

The differences observed between FLiP and FLiP-2 structural proteins lytic activity was quite surprizing. The results seem to indicate that FLiP-2 GP14 has less lytic activity in comparison with FLiP GP14 which could be hypothesized to be attributed to the two non-synonymous differences between these ORFs. Indeed, it is well known that just a single amino acid change can severely affect the activity of an enzyme or protein (Kalita et al. 2020; Ahammad et al. 2021). Such a conclusion cannot yet be made of course and would require both FLiP and FLiP-2 mutants where the substitutions would be swapped. Additionally, even though the same amount of protein was added into the wells, zymography is not a quantitative method to discriminate between the lytic activity of enzymes. To truly find out if the differences between the two enzymes lies in lytic activity, quantitative methods like the fluorescence-based hydrolysis assay employed by Chauhan et al. (2006).

Similarly interesting is the fact that these enzymes were only active in *E. coli* zymograms in cold temperatures. This result could be reflective of GP14 being cold adapted with efficient muralytic activity only occurring at low temperatures. Indeed some peptidoglycan hydrolases do seem to be equally or more active at low temperatures (Rydman and Bamford 2000; Orlando et al. 2020). If this were the case, this could partially explain the observation that FLiP and FLiP-2 do not efficiently lyse host cells in solution (Marjakangas. 2014; Mäkelä. 2019). Indeed, the muralytic activity of FLiP GP14 in cold treatment was previously shown by Mäkelä (2019). Ecologically, this would also be plausible given that lake Jyväsjärvi is a boreal lake that is frozen for several months of the year. Although an attractive hypothesis, this does not explain why GP14 could not degrade B330 peptidoglycan even though it comes from FLiPs main host and was demonstrated to do so both at RT and cold treatment in previous experiments (unpublished data). It is a possibility that the B330 peptidoglycan batch utilized for the zymogels was not optimal and thus the experiment with B330 zymogels should be repeated to confirm the result. In addition, the use of other assays with different mechanisms would be necessary to confirm these findings. These are intriguing set of results as they may hint at some aspects of FLiP ecology if proven true.

Although GP14 likely expressed difference in muralytic activity dependent on temperature, the second proposed lytic protein GP 7, produced a signal in all zymogels in all conditions with no major differences. Even though, GP 7 and GP 9 bands could not be differentiated on the gels likely since both these proteins are similar in size, it was previously shown that GP 7, not GP 9, was the lytic protein (Mäkelä. 2019). Following the logic mentioned above, this could be interpreted as GP 7 being active in all conditions meaning that *Finnlakevirus FLiP* has at least two muralytic enzymes, a pattern that to our knowledge is not seen in any other ssDNA phages. Mäkelä (2019) hypothesized that this may be indicative of *Finnlakevirus FLiP* having a holin-endolysin system similar to PRD1 and by extension being the first ssDNA phage with such a system. However, it is important to mention that zymogels can produce false positive results as some proteins thought to by lytic by zymography did not show such activity in solution-based methods. The false positive result is thought to result from proteins with high isoelectric points repelling the staining agent for zymography (Methylene blue) via electrostatic interactions, thus leaving an unstained region similar to peptidoglycan degradation (Escobar and Cross 2018). The fact that GP 7 has a high isoelectric point and was not predicted to have lytic activity (Laanto et al. 2017b) does make it at least possible for this to be the case. Given the novelty of discovering an ssDNA phage having a holin-endolysin system or even more than one lytic protein, it would be important to confirm the lytic activity of GP 7. To do this, first it would be beneficial to use the method employed by Escobar and Cross (2018) to see if the zymogram gives any false positives. Additionally, GP 7 would need to be purified either by overexpression in a model organism or purification from virions and tested separately by incubating the protein with

host and observe lysis or use a quantitative method as discussed above (Chauhan et al. 2006).

4.3 B330-P19 characterization and contrast to *Finnlakevirus FLiP*

The hypothesis that B330-P19 would be a tailed bacteriophage was proven to be correct from ORF annotations, TEM imaging and SDS-PAGE. Specifically, the two morphologies observed probably represent an intact virion and a virion that has contracted its tail and, in some cases, expelled its genome making it an empty capsid (e.g. Sørensen et al. 2015). This behaviour and the presence of a sheath protein among the annotated ORFs is the defining feature of a myophage as was discussed earlier (section 1.2). The large amount of structural proteins on the gel also argues for B330-P19 being a tailed phage as some myophages have been documented to have over 20 structural proteins (Clokie et al. 2008) befitting phages with such large genomes. However, a significant amount of the structural proteins observed in this analysis are probably leftovers from the host lysis given that linear gradient centrifugation in 5-20% sucrose used in this study does not exclude all host proteins. Despite the mentioned curiosity, the TEM clearly demonstrates that B330-P19 is a tailed phage with a myophage morphology.

The homology found between B330-P19 and cellulophaga phages phi17:2 and phi4:1 (isolated from the Baltic sea, Holmfeldt et al. 2013) is not too surprising given that the hosts of cellulophaga phages and flavobacterium phages are related in the family level (Bernardet and Nakagawa 2006). Despite this level of relatedness between the hosts, no other nucleotide similarities were detected between B330-P19 to other cellulophaga (or any other) phages by BLAST. The lack of homologous sequences together with the low annotation rate seem to indicate that B330-P19 is only a distant relative of select cellulophaga phages isolated by Holmfeldt et al. (2013). To find out how exactly B330-P19 is grouped relative to other phages, VirClust protein cluster trees could be constructed as was done in a previous study (Bartlau et al. 2022).

When comparing various aspects of both FLiP strains to B330-P19 not only are they genetically distinct, but B330-P19 phages also differ in their smaller, sharper-edged plaque morphologies, unsimilar host ranges and different life cycles. One key difference is the very high, burst size in comparison with both FLiP strains. Even though the calculated burst size is probably not true given the lack of a plateau phase as discussed earlier, the general shape of the curve also seems to point to fundamental differences between the life cycles in the assayed conditions. Indeed, the calculated burst size of B330-P19 is well within the range of typically reported burst sizes of dsDNA phages which can be between 10-150 (Uchiyama et al. 2008; Gallet et al. 2011; Manohar et al. 2019). Although the increased burst size may seem counterintuitive due to the smaller plaque size of B330-P19 compared to FLiP, it can be explained by the larger size and uneven shape of B330-P19 which would affect how the virion diffuses in the agar (see section 1.1). The large burst size also seems to suggest that unlike both FLiP strains, B330-P19 manages to lyse B330 more effectively both in liquid culture

and on agar plates. The infectious cycle difference is further evidenced by latent periods of the FLiP strains and B330-P19, which lasted between 180-200 and 215-235 min respectively. This timing difference is likely reflective of the different nature of the lysis timing mechanism that each phage evolved to have according to their niches (Wang et al. 2000; Bonachela et al. 2022). Taken together, the results from the one step growth curve seem to reflect the different infectious cycles of the phages and also suggest that the unusual non-lytic characteristics of the FLiP strains are a feature of *Finnlakevirus FLiP* and not a characteristic of B330 strain with all phages. These results also reflects the importance of studying non-model phages as the unusual life cycles may be caused underlying undiscovered molecular biology and may lead to impactful ecological dynamics in the environment (e.g. Thingstad and Lignell 1997; Knowles et al. 2016).

Interestingly, despite these large differences in life cycles between the two FLiP strains and B330-P19, the adsorption assay determined that none of the phages adsorbed effectively to B330. This is also interesting because the reasons behind the adsorption inefficiency for B330-P19 does not seem necessarily the same as for the two FLiP strains. Previously, I discussed that the reason for FLiP and FLiP-2 lack of adsorption may be the inefficiency of primary attachment to B330 as evidenced by the large supernatant fraction after bacterial pellet resuspension. However, in the case of B330-P19 the supernatant fraction taken after bacterial resuspension was considerably lower. This firstly may be an indication that B330-P19 has a stronger primary adsorption to B330 compared to both FLiP strains and that the cause for the low adsorption observed in the adsorption assay may be due to another reason entirely. Although this is the first-time performing adsorption assays on B330-P19, it is hard to imagine that it does not adsorb effectively given that most model myophages are known to adsorb well (Storms and Sauvageau 2014; Manohar et al. 2019). Furthermore, given that the adsorption of FLiP was less successful in B330 compared to previously (Mäkelä 2019), the low adsorption of B330-P19 now does not necessarily mean that it adsorbs poorly and could be due to a cryptic environmental variable. It is clear that the adsorption assays and one-step growth curves should be attempted again with different variations to see what the cause of the poor adsorption may be.

Although several structural proteins of B330-P19 were detected with SDS-PAGE, none of them seemed to have peptidoglycan degrading potential. This stands as stark contrast against the two FLiP virions which at least have one peptidoglycan degrading protein. At first this preliminary analysis may seem rather unusual given that, as mentioned in section 1.1, for the bacteriophage to inject its genome into the host, it must pass the peptidoglycan layer. In several tailed phages this is thought to be done by structural proteins on their tail which make a localized hole in the peptidoglycan (Moak and Molineux 2000; Kanamaru et al. 2002). However, some phages do not have muralytic enzymes on their virions or do not need them for entry (Moak and Molineux 2000; Rydman and Bamford 2000; Rodríguez-Rubio et al. 2013; Sun et al. 2014) and in some cases manage to make hollow protein tubes through the periplasm (Hu et al. 2013; Sun

et al. 2014). The interpretation that B330-P19 does not have an active muralytic enzyme structural protein can be contested however, given that ORF annotation leaves so many proteins un-annotated and the conditions in the zymogel may not be optimal for the lytic activity of the enzyme.

5 CONCLUSIONS

The first aim of this work characterizes the diversity of *Finnlakeviridae* phages by comparing their genetic identity and various life cycle phases of FLiP and FLiP-2. The second aim was to confirm the unusual phage-host interaction of FLiP by comparing it to B330-P19. The final aim was to characterize B330-P19 to find out what kind of bacteriophage it is. It was revealed that FLiP-2 was a strain of *Finnlakevirus FLiP*, thus strongly suggesting that the species has an established population either in lake Jyväsjärvi, the surrounding environment or both. Despite the close genetic relatedness, there were clear phenotypic differences between the phages expressed in host range and plaque morphology. Furthermore, several of the differences were transient during the study and is likely reflective of cryptic environmental factors rather than changes in FLiP-2 or B330 host. Although the exact mechanism for the phenotypic differences is not known, the muralytic activities of the structural proteins belonging to the FLiP strains differed and could be an underlying cause. However, the observed enzymatic differences would need to be confirmed with independent, quantitative methods. Despite the phenotypic differences between the FLiP strains, they still behaved similarly in their unusual life cycle characteristics. On the other hand, B330-P19, which was determined to be of myophage morphology, had divergent life cycle characteristics in comparison to both FLiP strains. This suggests that although several of FLiPs characteristics could not be replicated here, the overall unusual life cycle of FLiP is not expressed by the current representative of most studied phage type. It is vital to continue studying the life cycles and molecular biology of uncommon phage types like FLiP to understand viral diversity, their impact on ecosystems and learn more about uncharacterized molecular biology.

ACKNOWLEDGEMENTS

Thank you to the Emil Aaltonen foundation for the funding of this project. Special thanks to my mentors Lotta-Riina Sundberg, Elina Laanto and Kati Mäkelä for providing excellent advice and helping me through all the experiments and writing.

Jyväskylä May 15, 2023
Kim Kreuze

REFERENCES

Abby S.S., Cury J., Guglielmini J., Néron B., Touchon M. & Rocha E.P.C. 2016. Identification of protein secretion systems in bacterial genomes. *Scientific Reports* 6: 23080.

Abedon S.T. & Culler R.R. 2007a. Bacteriophage evolution given spatial constraint. *Journal of Theoretical Biology* 248: 111–119.

Abedon S.T. & Culler R.R. 2007b. Optimizing bacteriophage plaque fecundity. *Journal of Theoretical Biology* 249: 582–592.

Abedon S.T., Hyman P. & Thomas C. 2003. Experimental Examination of Bacteriophage Latent-Period Evolution as a Response to Bacterial Availability. *Applied and Environmental Microbiology* 69: 7499–7506.

Abedon S.T. & Yin J. 2009. Bacteriophage Plaques: Theory and Analysis. In: Clokie M.R.J. & Kropinski A.M. (eds.), *Methods in Molecular biology 501*. Humana Press New York, pp. 161-174

Ackermann H.-W., Roy R., Martin M., Murthy M.R.V. & Smirnoff W.A. 1978. Partial characterization of a cubic Bacillus phage. *Canadian Journal of Microbiology* 24: 986–993.

Adriaenssens E. & Brister J.R. 2017. How to Name and Classify Your Phage: An Informal Guide. *Viruses* 9: 70.

Aguado-García Y., Taboada B., Morán P., Rivera-Gutiérrez X., Serrano-Vázquez A., Iša P., Rojas-Velázquez L., Pérez-Juárez H., López S., Torres J., Ximénez C. & Arias C.F. 2020. Tobamoviruses can be frequently present in the oropharynx and gut of infants during their first year of life. *Scientific Reports* 10: 13595.

Ahammad T., Khan R.H., Sahu I.D., Drew D.L., Faul E., Li T., McCarrick R.M. & Lorigan G.A. 2021. Pinholin S21 mutations induce structural topology and conformational changes. *Biochimica et Biophysica Acta (BBA) - Biomembranes* 1863: 183771.

Aiewsakun P., Adriaenssens E.M., Lavigne R., Kropinski A.M. & Simmonds P. 2018. Evaluation of the genomic diversity of viruses infecting bacteria, archaea and eukaryotes using a common bioinformatic platform: steps towards a unified taxonomy. *Journal of General Virology* 99: 1331–1343.

Al-Shayeb B., Sachdeva R., Chen L.-X., Ward F., Munk P., Devoto A., Castelle C.J., Olm M.R., Bouma-Gregson K., Amano Y., He C., Méheust R., Brooks B., Thomas A., Lavy A., Matheus-Carnevali P., Sun C., Goltsman D.S.A., Borton M.A., Sharrar A., Jaffe A.L., Nelson T.C., Kantor R., Keren R., Lane K.R., Farag I.F., Lei S., Finstad K., Amundson R., Anantharaman K., Zhou J., Probst A.J., Power M.E., Tringe S.G., Li W.-J., Wrighton K., Harrison S., Morowitz M., Relman D.A., Doudna J.A., Lehours A.-C., Warren L., Cate J.H.D., Santini J.M. & Banfield J.F. 2020. Clades of huge phages from across Earth's ecosystems. *Nature* 578: 425–431.

Al-Shayeb B., Skopintsev P., Soczek K.M., Stahl E.C., Li Z., Groover E., Smock D., Eggers A.R., Pausch P., Cress B.F., Huang C.J., Staskawicz B., Savage D.F., Jacobsen S.E., Banfield J.F. & Doudna J.A. 2022. Diverse virus-encoded CRISPR-Cas systems include streamlined genome editors. *Cell* 185: 4574-4586.e16.

Altschul S.F., Gish W., Miller W., Myers E.W. & Lipman D.J. 1990. Basic Local Alignment Search Tool. *Journal of Molecular Biology* 215(3) 403-410.

Anderson T.F. 1949. The reactions of bacterial viruses with their host cells. *The Botanical Review* 15: 464–505.

Assimakopoulou I. 2022. Cellulophaga phage phi48:2 provides further evidence on icosahedral membrane-containing single-stranded DNA bacteriophages. Masters thesis.

Bailly-Bechet M., Vergassola M. & Rocha E. 2007. Causes for the intriguing presence of tRNAs in phages. *Genome Research* 17: 1486–1495.

Baranovskaya I., Sergeeva M., Fadeev A., Kadirova R., Ivanova A., Ramsay E. & Vasin A. 2019. Changes in RNA secondary structure affect NS1 protein expression during early stage influenza virus infection. *Virology Journal* 16: 162.

Bertani G. 1951. Studies on lysogenesis. I. The mode of phage liberation by lysogenic *Escherichia coli.* Journal of Bacteriology. 62(3): 293-300.

Barr J.J., Auro R., Furlan M., Whiteson K.L., Erb M.L., Pogliano J., Stotland A., Wolkowicz R., Cutting A.S., Doran K.S., Salamon P., Youle M. & Rohwer F. 2013. Bacteriophage adhering to mucus provide a non–host-derived immunity. *Proceedings of the National Academy of Sciences* 110: 10771–10776.

Bartlau N., Wichels A., Krohne G., Adriaenssens E.M., Heins A., Fuchs B.M., Amann R. & Moraru C. 2022. Highly diverse flavobacterial phages isolated from North Sea spring blooms. *The ISME Journal* 16: 555–568.

Bernardet J.-F. & Bowman J.P. 2006a. The Genus Flavobacterium. In: Dworkin M., Falkow S., Rosenberg E., Schleifer K.-H. & Stackebrandt E. (eds.), *The Prokaryotes: Volume 7: Proteobacteria: Delta, Epsilon Subclass*, Springer, New York, NY, pp. 481–531.

Bernardet J.-F. & Nakagawa Y. 2006b. An Introduction to the Family Flavobacteriaceae. In: Dworkin M., Falkow S., Rosenberg E., Schleifer K.-H. & Stackebrandt E. (eds.), *The Prokaryotes: Volume 7: Proteobacteria: Delta, Epsilon Subclass*, Springer, New York, New York, NY, pp. 455–480.

Besemer J. & Borodovsky M. 2005. GeneMark: web software for gene finding in prokaryotes, eukaryotes and viruses. *Nucleic Acids Research* 33: W451–W454.

Black L.W. 2015. Old, new, and widely true: The bacteriophage T4 DNA packaging mechanism. *Virology* 479–480: 650–656.

Bonachela J.A., Choua M. & Heath M.R. 2022. Unconstrained coevolution of bacterial size and the latent period of plastic phage Loverdo C. (ed.). *PLOS ONE* 17: e0268596.

Bradford M.M. 1976. A Rapid and Sensitive Method for the Quantitation of Microgram Quantities of Protein Utilizing the Principle of Protein-Dye Binding. *Analytical Biochemistry* 72: 248–254.

Cacciabue M., Currá A. & Gismondi M.I. 2019. ViralPlaque: a Fiji macro for automated assessment of viral plaque statistics. *PeerJ* 7: e7729.

Catalão M.J., Gil F., Moniz-Pereira J., São-José C. & Pimentel M. 2013. Diversity in bacterial lysis systems: bacteriophages show the way. *FEMS Microbiology Reviews* 37: 554–571.

Chamakura K. & Young R. 2019. Phage single-gene lysis: Finding the weak spot in the bacterial cell wall. *Journal of Biological Chemistry* 294: 3350–3358.

Chauhan A., Lofton H., Maloney E., Moore J., Fol M., Madiraju M.V.V.S. & Rajagopalan M. 2006. Interference of Mycobacterium tuberculosis cell division by Rv2719c, a cell wall hydrolase. *Molecular Microbiology* 62: 132–147.

Clokie M.R.J., Thalassinos K., Boulanger P., Slade S.E., Stoilova-McPhie S., Cane M., Scrivens J.H. & Mann N.H. 2008. A proteomic approach to the identification of the major virion structural proteins of the marine cyanomyovirus S-PM2. *Microbiology* 154: 1775–1782.

Couvin D., Bernheim A., Toffano-Nioche C., Touchon M., Michalik J., Néron B., Rocha E.P.C., Vergnaud G., Gautheret D. & Pourcel C. 2018. CRISPRCasFinder, an update of CRISRFinder, includes a portable version, enhanced performance and integrates search for Cas proteins. *Nucleic Acids Research* 46: W246–W251.

De Spiegeleer P., Sermon J., Lietaert A., Aertsen A. & Michiels C.W. 2004. Source of tryptone in growth medium affects oxidative stress resistance in Escherichia coli. *Journal of Applied Microbiology* 97: 124–133.

Dunn O.J. 1964. Multiple comparisons using rank sums. *Technometrics* 6(3): 241-252.

Eggers C.H. & Samuels D.S. 1999. Molecular Evidence for a New Bacteriophage of Borrelia burgdorferi. *Journal of Bacteriology* 181: 7308–7313.

Eiler A. & Bertilsson S. 2007. *Flavobacteria* Blooms in Four Eutrophic Lakes: Linking Population Dynamics of Freshwater Bacterioplankton to Resource Availability. *Applied and Environmental Microbiology* 73: 3511–3518.

Escobar C.A. & Cross T.A. 2018. False positives in using the zymogram assay for identification of peptidoglycan hydrolases. *Analytical Biochemistry* 543: 162–166.

Espejo R.T. & Canelo E.S. 1968. Properties of bacteriophage PM2: a lipid-containing bacterial virus. *Virology* 34: 738–747.

Espejo R.T., Canelo E.S. & Sinsheimer R.L. 1969. DNA OF BACTERIOPHAGE PM2: A CLOSED CIRCULAR DOUBLE-STRANDED MOLECULE. *Proceedings of the National Academy of Sciences of the United States of America* 63: 1164–1168.

Fernandes S. & São-José C. 2018. Enzymes and Mechanisms Employed by Tailed Bacteriophages to Breach the Bacterial Cell Barriers. *Viruses* 10: 396.

Finn R.D., Clements J. & Eddy S.R. 2011. HMMER web server: interactive sequence similarity searching. *Nucleic Acids Research* 39: W29–W37.

Fokine A. & Rossmann M.G. 2014. Molecular architecture of tailed double-stranded DNA phages. *Bacteriophage* 4: e28281.

Fuhrman J.A. 1999. Marine viruses and their biogeochemical and ecological effects. *Nature* 399: 541–548.

Gallet R., Kannoly S. & Wang I.-N. 2011. Effects of bacteriophage traits on plaque formation. *BMC Microbiology* 11: 181.

Garneau J.R., Depardieu F., Fortier L.-C., Bikard D. & Monot M. 2017. PhageTerm: a tool for fast and accurate determination of phage termini and packaging mechanism using next-generation sequencing data. *Scientific Reports* 7: 8292.

Goddard V., Baker A., Davy J., Adams D., De Ville M., Thackeray S., Maberly S. & Wilson W. 2005. Temporal distribution of viruses, bacteria and phytoplankton throughout the water column in a freshwater hypereutrophic lake. *Aquatic Microbial Ecology* 39: 211–223.

Goldsmith D., Brum J., Hopkins M., Carlson C. & Breitbart M. 2015. Water column stratification structures viral community composition in the Sargasso Sea. *Aquatic Microbial Ecology* 76: 85–94.

Gómez P. & Buckling A. 2011. Bacteria-Phage Antagonistic Coevolution in Soil. *Science* 332: 106–109.

Gong Q., Wang X., Huang H., Sun Y., Qian X., Xue F., Ren J., Dai J. & Tang F. 2021. Novel Host Recognition Mechanism of the K1 Capsule-Specific Phage of *Escherichia coli* : Capsular Polysaccharide as the First Receptor and Lipopolysaccharide as the Secondary Receptor Pfeiffer J.K. (ed.). *Journal of Virology* 95: e00920-21.

Gorasia D.G., Veith P.D. & Reynolds E.C. 2020. The Type IX Secretion System: Advances in Structure, Function and Organisation. *Microorganisms* 8: 1173.

Hattman S. & Fukusawa T. 1963. Host-induced modification of T-even phages due to defective glucosylation of their DNA. *Proceedings of the National Academy of Sciences of the United States of America* 50(2): 297-300.

Haider S.R., Reid H.J. & Sharp B.L. 2012. Tricine-SDS-PAGE. *Methods in molecular biology* 869: 81-91.

Hayashi T., Baba T., Matsumoto H. & Terawaki Y. 1990. Phage-conversion of cytotoxin production in Pseudomonas aeruginosa. *Molecular Microbiology* 4: 1703–1709.

He M., Cai L., Zhang C., Jiao N. & Zhang R. 2017. Phylogenetic Diversity of T4-Type Phages in Sediments from the Subtropical Pearl River Estuary. *Frontiers in Microbiology* 8: 897.

Hendrix R.W., Smith M.C.M., Burns R.N., Ford M.E. & Hatfull G.F. 1999. Evolutionary relationships among diverse bacteriophages and prophages: All the world's a phage. *Proceedings of the National Academy of Sciences* 96: 2192–2197.

Holmfeldt K., Solonenko N., Shah M., Corrier K., Riemann L., VerBerkmoes N.C. & Sullivan M.B. 2013. Twelve previously unknown phage genera are ubiquitous in global oceans. *Proceedings of the National Academy of Sciences* 110: 12798–12803.

Holt R.A., Amandi A., Rohovec J.S. & Fryer J.L. 1989. Relation of water temperature to bacterial coldwater disease in coho salmon, chinook salmon and rainbow trout. *Journal of Aquatic Animal Health* 1:94-101.

Hu B., Margolin W., Molineux I.J. & Liu J. 2013. The Bacteriophage T7 Virion Undergoes Extensive Structural Remodeling During Infection. *Science* 339: 576–579.

Hyman P. & Abedon S.T. 2009. Practical Methods for Determining Phage Growth Parameters. In: Clokie M.R.J. & Kropinski A.M. (eds.), *Methods in Molecular biology 501*. Humana Press New York, pp. 175-202.

Inomata T., Kimura H., Hayasaka H., Shiozaki A., Fujita Y. & Kashiwagi A. 2012. Quantitative comparison of the RNA bacteriophage Qβ infection cycle in rich and minimal media. *Archives of Virology* 157: 2163–2169.

Jinek M., Chylinski K., Fonfara I., Hauer M., Doudna J.A. & Charpentier E. 2012. A Programmable Dual-RNA–Guided DNA Endonuclease in Adaptive Bacterial Immunity. *Science* 337: 816–821.

Kalita J., Shukla H. & Tripathi T. 2020. Engineering glutathione S-transferase with a point mutation at conserved F136 residue increases the xenobiotic-metabolizing activity. *International Journal of Biological Macromolecules* 163: 1117–1126.

Kanamaru S., Leiman P.G., Kostyuchenko V.A., Chipman P.R., Mesyanzhinov V.V., Arisaka F. & Rossmann M.G. 2002. Structure of the cell-puncturing device of bacteriophage T4. *Nature* 415: 553–557.

Kauffman K.M., Hussain F.A., Yang J., Arevalo P., Brown J.M., Chang W.K., VanInsberghe D., Elsherbini J., Sharma R.S., Cutler M.B., Kelly L. & Polz M.F. 2018. A major lineage of non-tailed dsDNA viruses as unrecognized killers of marine bacteria. *Nature* 554: 118–122.

Kejzar N., Laanto E., Rissanen I., Abrishami V., Selvaraj M., Moineau S., Ravantti J., Sundberg L.-R. & Huiskonen J.T. 2022. Cryo-EM structure of ssDNA bacteriophage ΦCjT23 provides insight into early virus evolution. *Nature Communications* 13: 7478.

Kershner J.P., Yu McLoughlin S., Kim J., Morgenthaler A., Ebmeier C.C., Old W.M. & Copley S.D. 2016. A Synonymous Mutation Upstream of the Gene Encoding a Weak-Link Enzyme Causes an Ultrasensitive Response in Growth Rate Metcalf W.W. (ed.). *Journal of Bacteriology* 198: 2853–2863.

Kinouchi M. & Kurokawa K. 2006. tRNAfinder: A Software System To Find All tRNA Genes in the DNA Sequence Based on the Cloverleaf Secondary Structure. *Journal of Computer Aided Chemistry* 7: 116-124.

Knowles B., Silveira C.B., Bailey B.A., Barott K., Cantu V.A., Cobián-Güemes A.G., Coutinho F.H., Dinsdale E.A., Felts B., Furby K.A., George E.E., Green K.T., Gregoracci G.B., Haas A.F., Haggerty J.M., Hester E.R., Hisakawa N., Kelly L.W., Lim Y.W., Little M., Luque A., McDole-Somera T., McNair K., De Oliveira L.S., Quistad S.D., Robinett N.L., Sala E., Salamon P., Sanchez S.E., Sandin S., Silva G.G.Z., Smith J., Sullivan C., Thompson C., Vermeij M.J.A., Youle M., Young C., Zgliczynski B., Brainard R., Edwards R.A., Nulton J., Thompson F.

& Rohwer F. 2016. Lytic to temperate switching of viral communities. *Nature* 531: 466–470.

Koonin E.V., Dolja V.V., Krupovic M., Varsani A., Wolf Y.I., Yutin N., Zerbini F.M. & Kuhn J.H. 2020. Global Organization and Proposed Megataxonomy of the Virus World. *Microbiology and Molecular Biology Reviews* 84: e00061-19.

Kortright K.E., Chan B.K., Evans B.R. & Turner P.E. 2022. Arms race and fluctuating selection dynamics in *Pseudomonas aeruginosa* bacteria coevolving with phage OMKO1. *Journal of Evolutionary Biology* 35: 1475–1487.

Kropinski A.M. 2009. Measurement of the Rate of Attachment of Bacteriophage to Cells. In: Clokie M.R.J. & Kropinski A.M. (eds.), *Methods in Molecular biology 501*. Humana Press New York, pp. 151-155.

Krupovič M. & Bamford D.H. 2007. Putative prophages related to lytic tailless marine dsDNA phage PM2 are widespread in the genomes of aquatic bacteria. *BMC Genomics* 8: 236.

Laanto E., Hoikkala V., Ravantti J. & Sundberg L.-R. 2017a. Long-term genomic coevolution of host-parasite interaction in the natural environment. *Nature Communications* 8: 111.

Laanto E., Mäntynen S., De Colibus L., Marjakangas J., Gillum A., Stuart D.I., Ravantti J.J., Huiskonen J.T. & Sundberg L.-R. 2017b. Virus found in a boreal lake links ssDNA and dsDNA viruses. *Proceedings of the National Academy of Sciences of the United States of America* 114: 8378–8383.

Laanto E., Sundberg L.-R. & Bamford J.K.H. 2011. Phage Specificity of the Freshwater Fish Pathogen Flavobacterium columnare▿. *Applied and Environmental Microbiology* 77: 7868–7872.

Lederberg E.M. & Lederberg J. 1953. GENETIC STUDIES OF LYSOGENICITY IN ESCHERICHIA COLI. *Genetics* 38: 51–64.

Lin D.M., Koskella B. & Lin H.C. 2017. Phage therapy: An alternative to antibiotics in the age of multi-drug resistance. *World Journal of Gastrointestinal Pharmacology and Therapeutics* 8: 162–173.

Lunde M., Blatny J.M., Lillehaug D., Aastveit A.H. & Nes I.F. 2003. Use of real-time quantitative PCR for the analysis of phiLC3 prophage stability in lactococci. *Applied and Environmental Microbiology* 69: 41–48.

Manohar P., Tamhankar A.J., Lundborg C.S. & Nachimuthu R. 2019. Therapeutic Characterization and Efficacy of Bacteriophage Cocktails Infecting Escherichia coli, Klebsiella pneumoniae, and Enterobacter Species. *Frontiers in Microbiology* 10: 574.

Marjakangas J. 2014. Flavobakteereita infektoivan ssDNA bakteriofagi V155:n karakterisointi. Masters thesis.

Mäkelä K. 2019. Flavobakteereja infektoivan ssDNA-faagi FLiP:n isäntävuorovaikutukset. Masters thesis.

Mäntynen S., Laanto E., Sundberg L.-R., Poranen M.M., Oksanen H.M. & Report Consortium I. 2020. ICTV Virus Taxonomy Profile: Finnlakeviridae. *The Journal of General Virology* 101: 894–895.

Mäntynen S., Sundberg L.-R., Oksanen H.M. & Poranen M.M. 2019. Half a Century of Research on Membrane-Containing Bacteriophages: Bringing New Concepts to Modern Virology. *Viruses* 11: 76.

McBride M.J. & Zhu Y. 2013. Gliding Motility and Por Secretion System Genes Are Widespread among Members of the Phylum Bacteroidetes. *Journal of Bacteriology* 195: 270–278.

Mistry J., Chuguransky S., Williams L., Qureshi M., Salazar G.A., Sonnhammer E.L.L., Tosatto S.C.E., Paladin L., Raj S., Richardson L.J., Finn R.D. & Bateman A. 2021. Pfam: The protein families database in 2021. *Nucleic Acids Research* 49: D412–D419.

Moak M. & Molineux I.J. 2000. Role of the Gp16 lytic transglycosylase motif in bacteriophage T7 virions at the initiation of infection. *Molecular Microbiology* 37: 345–355.

Moldovan R., Chapman-McQuiston E. & Wu X.L. 2007. On Kinetics of Phage Adsorption. *Biophysical Journal* 93: 303–315.

Muhire B.M., Golden M., Murrell B., Lefeuvre P., Lett J.-M., Gray A., Poon A.Y.F., Ngandu N.K., Semegni Y., Tanov E.P., Monjane A.L., Harkins G.W., Varsani A., Shepherd D.N. & Martin D.P. 2014. Evidence of Pervasive Biologically Functional Secondary Structures within the Genomes of Eukaryotic Single-Stranded DNA Viruses. *Journal of Virology* 88: 1972–1989.

Mushegian A.R. 2020. Are There 1031 Virus Particles on Earth, or More, or Fewer? *Journal of Bacteriology* 202: e00052-20.

Nilsson E., Bayfield O.W., Lundin D., Antson A.A. & Holmfeldt K. 2020. Diversity and Host Interactions among Virulent and Temperate Baltic Sea Flavobacterium Phages. *Viruses* 12: 158.

Olsen R.H., Siak J.S. & Gray R.H. 1974. Characteristics of PRD1, a plasmid-dependent broad host range DNA bacteriophage. *Journal of Virology* 14: 689–699.

Orlando M., Pucciarelli S. & Lotti M. 2020. Endolysins from Antarctic Pseudomonas Display Lysozyme Activity at Low Temperature. *Marine Drugs* 18: 579.

Parena A.J.S., Silva B.B.I., Mercado R.M.L., Sendon A.A.A., Signabon F.B., Balidion J.F. & Encabo J.R. 2022. Lytic phages display protective effects against soft rot-causing *Pectobacterium* sp. *Biocontrol Science and Technology* 32: 1326–1345.

Paysan-Lafosse T., Blum M., Chuguransky S., Grego T., Pinto B.L., Salazar G.A., Bileschi M.L., Bork P., Bridge A., Colwell L., Gough J., Haft D.H., Letunić I., Marchler-Bauer A., Mi H., Natale D.A., Orengo C.A., Pandurangan A.P., Rivoire C., Sigrist C.J.A., Sillitoe I., Thanki N., Thomas P.D., Tosatto S.C.E., Wu C.H. & Bateman A. 2023. InterPro in 2022. *Nucleic Acids Research* 51: D418–D427.

Peralta B., Gil-Carton D., Castaño-Díez D., Bertin A., Boulogne C., Oksanen H.M., Bamford D.H. & Abrescia N.G.A. 2013. Mechanism of Membranous Tunnelling Nanotube Formation in Viral Genome Delivery Rey F.A. (ed.). *PLoS Biology* 11: e1001667.

Qin X., Sun Q., Yang B., Pan X., He Y. & Yang H. 2017. Quorum sensing influences phage infection efficiency via affecting cell population and

physiological state: Quorum sensing influences phage infection efficiency. *Journal of Basic Microbiology* 57: 162–170.

Rakhuba D.V., Kolomiets E.I., Dey E.S. & Novik G.I. 2010. Bacteriophage receptors, mechanisms of phage adsorption and penetration into host cell. *Polish Journal of Microbiology* 59: 145–155.

Rao V.B. & Feiss M. 2008. The Bacteriophage DNA Packaging Motor. *Annual Review of Genetics* 42: 647–681.

Richter C.A. & Pate J.L. 1988. Temperate phages and bacteriocins of the gliding bacterium *Cytophaga johnsonae*. *Journal of general microbiology* 134(2): 253-261.

Rodríguez-Rubio L., Quiles-Puchalt N., Martínez B., Rodríguez A., Penadés J.R. & García P. 2013. The Peptidoglycan Hydrolase of Staphylococcus aureus Bacteriophage ϕ11 Plays a Structural Role in the Viral Particle. *Applied and Environmental Microbiology* 79: 6187–6190.

Rohwer F. & Edwards R. 2002. The Phage Proteomic Tree: a Genome-Based Taxonomy for Phage. *Journal of Bacteriology* 184: 4529–4535.

Rojano-Nisimura A.M., Haning K., Janovsky J., Vasquez K.A., Thompson J.P. & Contreras L.M. 2020. Codon Selection Affects Recruitment of Ribosome-Associating Factors during Translation. *ACS Synthetic Biology* 9: 329–342.

Rostøl J.T. & Marraffini L. 2019. (Ph)ighting Phages: How Bacteria Resist Their Parasites. *Cell Host & Microbe* 25: 184–194.

Roux S., Krupovic M., Poulet A., Debroas D. & Enault F. 2012. Evolution and Diversity of the Microviridae Viral Family through a Collection of 81 New Complete Genomes Assembled from Virome Reads Dutilh B.E. (ed.). *PLoS ONE* 7: e40418.

Roznowski A.P., Young R.J., Love S.D., Andromita A.A., Guzman V.A., Wilch M.H., Block A., McGill A., Lavelle M., Romanova A., Sekiguchi A., Wang M., Burch A.D. & Fane B.A. 2019. Recessive Host Range Mutants and Unsusceptible Cells That Inactivate Virions without Genome Penetration: Ecological and Technical Implications Sandri-Goldin R.M. (ed.). *Journal of Virology* 93: e01767-18.

Rydman P.S. & Bamford D.H. 2000. Bacteriophage PRD1 DNA entry uses a viral membrane-associated transglycosylase activity. *Molecular Microbiology* 37: 356–363.

Salzberg S.L., Delcher A.L., Kasif S. & White O. 1998. Microbial gene identification using interpolated Markov models. *Nucleic Acids Research* 26: 544–548.

Santos-Pérez I., Charro D., Gil-Carton D., Azkargorta M., Elortza F., Bamford D.H., Oksanen H.M. & Abrescia N.G.A. 2019. Structural basis for assembly of vertical single β-barrel viruses. *Nature Communications* 10: 1184.

Schindelin J., Arganda-Carreras I., Frise E., Kaynig V., Longair M., Pietzsch T., Preibisch S., Rueden C., Saalfeld S., Schmid B., Tinevez J.-Y., White D.J., Hartenstein V., Eliceiri K., Tomancak P. & Cardona A. 2012. Fiji: an open-source platform for biological-image analysis. *Nature Methods* 9: 676–682.

Seong H.J., Roux S., Hwang C.Y. & Sul W.J. 2022. Marine DNA methylation patterns are associated with microbial community composition and inform virus-host dynamics. *Microbiome* 10: 157.

Shieh H.S. 1980. Studies on the nutrition of a fish pathogen, *Flexibacter columnaris*. *Microbios Letters* 13(51/52): 129-133

Shkoporov A.N., Khokhlova E.V., Fitzgerald C.B., Stockdale S.R., Draper L.A., Ross R.P. & Hill C. 2018. ΦCrAss001 represents the most abundant bacteriophage family in the human gut and infects Bacteroides intestinalis. *Nature Communications* 9: 4781.

Sioud M. 2019. Phage Display Libraries: From Binders to Targeted Drug Delivery and Human Therapeutics. *Molecular Biotechnology* 61: 286–303.

Smith K. 2019. The effects of growth medium on *Flavobacterium columnare* colony morphology and its phage resistance mechanisms. Masters thesis.

Sørensen M.C.H., Gencay Y.E., Birk T., Baldvinsson S.B., Jäckel C., Hammerl J.A., Vegge C.S., Neve H. & Brøndsted L. 2015. Primary Isolation Strain Determines Both Phage Type and Receptors Recognised by Campylobacter jejuni Bacteriophages Van Raaij M.J. (ed.). *PLOS ONE* 10: e0116287.

Stanier R.Y. 1947. Studies on nonfruiting myxobacteria; *Cytophaga johnsonae*, n. sp., a chitin decomposing myxobacterium. *Journal of bacteriology* 53(3) 297-315.

Sternberg N. & Austin S. 1981. The maintenance of the P1 plasmid prophage. *Plasmid* 5: 20–31.

Storms Z.J. & Sauvageau D. 2014. Evidence That the Heterogeneity of a T4 Population Is the Result of Heritable Traits Schuch R. (ed.). *PLoS ONE* 9: e116235.

Storms Z.J. & Sauvageau D. 2015. Modeling tailed bacteriophage adsorption: Insight into mechanisms. *Virology* 485: 355–362.

Strömsten N.J., Bamford D.H. & Bamford J.K.H. 2003. The Unique Vertex of Bacterial Virus PRD1 Is Connected to the Viral Internal Membrane. *Journal of Virology* 77: 6314–6321.

Sun L., Young L.N., Zhang X., Boudko S.P., Fokine A., Zbornik E., Roznowski A.P., Molineux I.J., Rossmann M.G. & Fane B.A. 2014. Icosahedral bacteriophage ΦX174 forms a tail for DNA transport during infection. *Nature* 505: 432–435.

Székely A.J. & Breitbart M. 2016. Single-stranded DNA phages: from early molecular biology tools to recent revolutions in environmental microbiology. *FEMS Microbiology Letters* 363: fnw027.

Terzian P., Olo Ndela E., Galiez C., Lossouarn J., Pérez Bucio R.E., Mom R., Toussaint A., Petit M.-A. & Enault F. 2021. PHROG: families of prokaryotic virus proteins clustered using remote homology. *NAR Genomics and Bioinformatics* 3: lqab067.

The Galaxy Community, Afgan E., Nekrutenko A., Grüning B.A., Blankenberg D., Goecks J., Schatz M.C., Ostrovsky A.E., Mahmoud A., Lonie A.J., Syme A., Fouilloux A., Bretaudeau A., Nekrutenko A., Kumar A., Eschenlauer A.C., DeSanto A.D., Guerler A., Serrano-Solano B., Batut B., Grüning B.A., Langhorst B.W., Carr B., Raubenolt B.A., Hyde C.J., Bromhead C.J., Barnett C.B., Royaux C., Gallardo C., Blankenberg D., Fornika D.J., Baker D., Bouvier D.,

Clements D., De Lima Morais D.A., Tabernero D.L., Lariviere D., Nasr E., Afgan E., Zambelli F., Heyl F., Psomopoulos F., Coppens F., Price G.R., Cuccuru G., Corguillé G.L., Von Kuster G., Akbulut G.G., Rasche H., Hotz H.-R., Eguinoa I., Makunin I., Ranawaka I.J., Taylor J.P., Joshi J., Hillman-Jackson J., Goecks J., Chilton J.M., Kamali K., Suderman K., Poterlowicz K., Yvan L.B., Lopez-Delisle L., Sargent L., Bassetti M.E., Tangaro M.A., Van Den Beek M., Čech M., Bernt M., Fahrner M., Tekman M., Föll M.C., Schatz M.C., Crusoe M.R., Roncoroni M., Kucher N., Coraor N., Stoler N., Rhodes N., Soranzo N., Pinter N., Goonasekera N.A., Moreno P.A., Videm P., Melanie P., Mandreoli P., Jagtap P.D., Gu Q., Weber R.J.M., Lazarus R., Vorderman R.H.P., Hiltemann S., Golitsynskiy S., Garg S., Bray S.A., Gladman S.L., Leo S., Mehta S.P., et al. 2022. The Galaxy platform for accessible, reproducible and collaborative biomedical analyses: 2022 update. *Nucleic Acids Research* 50: W345–W351.

The UniProt Consortium, Bateman A., Martin M.-J., Orchard S., Magrane M., Agivetova R., Ahmad S., Alpi E., Bowler-Barnett E.H., Britto R., Bursteinas B., Bye-A-Jee H., Coetzee R., Cukura A., Da Silva A., Denny P., Dogan T., Ebenezer T., Fan J., Castro L.G., Garmiri P., Georghiou G., Gonzales L., Hatton-Ellis E., Hussein A., Ignatchenko A., Insana G., Ishtiaq R., Jokinen P., Joshi V., Jyothi D., Lock A., Lopez R., Luciani A., Luo J., Lussi Y., MacDougall A., Madeira F., Mahmoudy M., Menchi M., Mishra A., Moulang K., Nightingale A., Oliveira C.S., Pundir S., Qi G., Raj S., Rice D., Lopez M.R., Saidi R., Sampson J., Sawford T., Speretta E., Turner E., Tyagi N., Vasudev P., Volynkin V., Warner K., Watkins X., Zaru R., Zellner H., Bridge A., Poux S., Redaschi N., Aimo L., Argoud-Puy G., Auchincloss A., Axelsen K., Bansal P., Baratin D., Blatter M.-C., Bolleman J., Boutet E., Breuza L., Casals-Casas C., De Castro E., Echioukh K.C., Coudert E., Cuche B., Doche M., Dornevil D., Estreicher A., Famiglietti M.L., Feuermann M., Gasteiger E., Gehant S., Gerritsen V., Gos A., Gruaz-Gumowski N., Hinz U., Hulo C., Hyka-Nouspikel N., Jungo F., Keller G., Kerhornou A., Lara V., Le Mercier P., Lieberherr D., et al. 2021. UniProt: the universal protein knowledgebase in 2021. *Nucleic Acids Research* 49: D480–D489.

Thingstad T. & Lignell R. 1997. Theoretical models for the control of bacterial growth rate, abundance, diversity and carbon demand. *Aquatic Microbial Ecology* 13: 19–27.

Tisza M.J., Pastrana D.V., Welch N.L., Stewart B., Peretti A., Starrett G.J., Pang Y.-Y.S., Krishnamurthy S.R., Pesavento P.A., McDermott D.H., Murphy P.M., Whited J.L., Miller B., Brenchley J., Rosshart S.P., Rehermann B., Doorbar J., Ta'ala B.A., Pletnikova O., Troncoso J.C., Resnick S.M., Bolduc B., Sullivan M.B., Varsani A., Segall A.M. & Buck C.B. 2020. Discovery of several thousand highly diverse circular DNA viruses. *eLife* 9: e51971.

Turki S., Kraeim I.B., Weeckers F., Thonart P. & Kallel H. 2009. Isolation of bioactive peptides from tryptone that modulate lipase production in Yarrowia lipolytica. *Bioresource Technology* 100: 2724–2731.

Turner D., Shkoporov A.N., Lood C., Millard A.D., Dutilh B.E., Alfenas-Zerbini P., Van Zyl L.J., Aziz R.K., Oksanen H.M., Poranen M.M., Kropinski A.M., Barylski J., Brister J.R., Chanisvili N., Edwards R.A., Enault F., Gillis A., Knezevic

P., Krupovic M., Kurtböke I., Kushkina A., Lavigne R., Lehman S., Lobocka M., Moraru C., Moreno Switt A., Morozova V., Nakavuma J., Reyes Muñoz A., Rūmnieks J., Sarkar B., Sullivan M.B., Uchiyama J., Wittmann J., Yigang T. & Adriaenssens E.M. 2023. Abolishment of morphology-based taxa and change to binomial species names: 2022 taxonomy update of the ICTV bacterial viruses subcommittee. *Archives of Virology* 168: 74.

Uchiyama J., Rashel M., Maeda Y., Takemura I., Sugihara S., Akechi K., Muraoka A., Wakiguchi H. & Matsuzaki S. 2008. Isolation and characterization of a novel *Enterococcus faecalis* bacteriophage φEF24C as a therapeutic candidate. *FEMS Microbiology Letters* 278: 200–206.

Vandamme E.J. & Mortelmans K. 2019. A century of bacteriophage research and applications: impacts on biotechnology, health, ecology and the economy!: A century of bacteriophage research and applications. *Journal of Chemical Technology & Biotechnology* 94: 323–342.

Wang Y., Fan H. & Tong Y. 2023. Unveil the Secret of the Bacteria and Phage Arms Race. *International Journal of Molecular Sciences* 24: 4363.

Wang X., Kim Y., Ma Q., Hong S.H., Pokusaeva K., Sturino J.M. & Wood T.K. 2010. Cryptic prophages help bacteria cope with adverse environments. *Nature Communications* 1: 147.

Wang I.-N., Smith D.L. & Young R. 2000. Holins: The Protein Clocks of Bacteriophage Infections. *Annual Review of Microbiology* 54: 799–825.

Weiss S.B., Hsu W.T., Foft J.W. & Scherberg N.H. 1968. Transfer RNA coded by the T4 bacteriophage genome. *Proceedings of the National Academy of Sciences of the United States of America.* 61(1): 114-21

Winter C., Kerros M.-E. & Weinbauer M.G. 2009. Seasonal and depth-related dynamics of prokaryotes and viruses in surface and deep waters of the northwestern Mediterranean Sea. *Deep Sea Research Part I: Oceanographic Research Papers* 56: 1972–1982.

Xu L., Bao L., Deng W., Zhu H., Li F., Chen T., Lv Q., Yuan J., Xu Y., Li Y., Yao Y., Gu S., Yu P., Chen H. & Qin C. 2014. Rapid adaptation of avian H7N9 virus in pigs. *Virology* 452–453: 231–236.

Yin J. & McCaskill J.S. 1992. Replication of viruses in a growing plaque: a reaction-diffusion model. *Biophysical Journal* 61: 1540–1549.

Yutin N., Bäckström D., Ettema T.J.G., Krupovic M. & Koonin E.V. 2018. Vast diversity of prokaryotic virus genomes encoding double jelly-roll major capsid proteins uncovered by genomic and metagenomic sequence analysis. *Virology Journal* 15: 67.

Zhang M., Wang Y., Chen J., Hong X., Xu X., Wu Z., Ahmed T., Loh B., Leptihn S., Hassan S., Hassan M.M., Sun G. & Li B. 2022. Identification and Characterization of a New Type of Holin-Endolysin Lysis Cassette in Acidovorax oryzae Phage AP1. *Viruses* 14: 167.

Zhou N., Park K. & Dybvig K. 1995. Mycoplasma virus P1 has a linear, double-stranded DNA genome with inverted terminal repeats. *Plasmid* 33: 41–49.

Zuppi M., Hendrickson H.L., O'Sullivan J.M. & Vatanen T. 2022. Phages in the Gut Ecosystem. *Frontiers in Cellular and Infection Microbiology* 11: 822562.

APPENDIX 1. PRIMER INFORMATION

FLiP MCP Forward primer
GAA TGT TGT TCG CGG TGC TT

FLiP MCP Reverse primer
AGA ATC AAC CTC GTT CGC GT

FLiP RiP Forward primer
TCA GCG CAA AGG TTA GCC AT

FLiP RiP Reverse primer
GCT GTG CTA ACG CCC AAA TC

APPENDIX 2. SDS-PAGE AND ZYMOGRAM BUFFERS AND RECIEPES

Buffers:

Buffer IIa: 3 M Trizma base (Sigma, USA) pH 8.7.
Buffer IIb: 0.5 M Trizma base, 0.5 M NaH_2PO_4 pH 7.8.
3X sample buffer: 10 ml buffer IIa, 10 ml 10% SDS (Sigma, Germany); 0.4 ml 0.5 M EDTA (pH 7.5), 1 ml mercaptoethanol, 10 ml 87% glycerol and 10 mg bromophenol blue.
Tricine SDS-PAGE cathode buffer: 0.1 M Trizma base, 0.1 M Tricine (Thermo Fischer, USA), 0.1% SDS, pH 8.25.
Tricine SDS-PAGE anode buffer: 0.2 M Tris-base pH 8.9

Large Tricine SDS-PAGE gels:

Tricine SDS-PAGE loading gel 5%: 1.7 ml 30% acrylamide, 2.5 ml IIb buffer, 5.8 ml dH2O, 10 µl tetramethylenediamine (TEMED), 100 µl 10% ammonium persulfate (APS).
Tricine SDS-PAGE running gel 17%: 14.9 ml 40% acrylamide, 4.6 g 87% glycerol, 11.6 ml IIa buffer, 4.5 ml dH2O, 12 µl TEMED, 117 µl 10% APS.

Small Tricine SDS-PAGE gels:

Tricine SDS-PAGE loading gel 5%: 1.7 ml 30% acrylamide, 2.5 ml IIb buffer, 5.8 ml dH2O, 10 µl TEMED, 100 µl 10% APS.
Tricine SDS-PAGE running gel 17%: 4.95 ml 40% acrylamide, 1.5 g 87% glycerol, 3.9 ml IIa buffer, 1.95 ml dH2O, 4 µl TEMED, 40 µl 10% APS.
Zymogels 17%: 4.95 ml 40% acrylamide, 1.5 g 87% glycerol, 3.9 ml IIa buffer, 1.5 ml sonicated B330 or *E. coli* peptidoglycan, 0.45 ml dH2O, 4 µl TEMED, 40 µl 10% APS.

APPENDIX 3: POSITIONS, LENGTHS AND ANNOTATIONS OF B330-P19 PREDICTED ORFS

ORF name	Start position in genome	End position in genome	ORF length (bp)	Direction	Annotation
ORF1	315	1751	1437	reverse	Hypothetical protein
ORF2	2026	2301	276	reverse	Hypothetical protein
ORF3	2294	2677	384	reverse	Hypothetical protein
ORF4	2677	2889	213	reverse	Hypothetical protein
ORF5	2897	3757	861	reverse	Hypothetical protein
ORF6	3934	4176	243	reverse	Hypothetical protein
ORF7	4193	4492	300	reverse	Hypothetical protein
ORF8	4496	4789	294	reverse	Hypothetical protein
ORF9	4797	5054	258	reverse	Hypothetical protein
ORF10	5065	5343	279	reverse	Hypothetical protein
ORF11	5345	5608	264	reverse	Hypothetical protein
ORF12	5608	6369	762	reverse	Hypothetical protein
ORF13	6436	6630	195	reverse	Hypothetical protein
ORF14	6633	6935	303	reverse	Hypothetical protein
ORF15	6925	7179	255	reverse	Hypothetical protein
ORF16	7182	7718	537	reverse	Hypothetical protein
ORF17	7708	9531	1824	reverse	Hypothetical protein
ORF18	9873	10094	222	reverse	Hypothetical protein
ORF19	10091	10420	330	reverse	Hypothetical protein
ORF20	10469	10615	147	reverse	Hypothetical protein
ORF21	10666	10827	162	reverse	Hypothetical protein
ORF22	11109	11309	201	reverse	Hypothetical protein
ORF23	11306	11575	270	reverse	Hypothetical protein
ORF24	11721	11915	195	reverse	Hypothetical protein
ORF25	11918	12472	555	reverse	Hypothetical protein
ORF26	12472	12984	513	reverse	Hypothetical protein
ORF27	13040	13699	660	reverse	Hypothetical protein
ORF28	13696	14133	438	reverse	Hypothetical protein
ORF29	14109	14396	288	reverse	Hypothetical protein
ORF30	14425	14715	291	reverse	Hypothetical protein
ORF31	14771	15205	435	reverse	Hypothetical protein
ORF32	15217	15321	105	reverse	Hypothetical protein
ORF33	15305	15808	504	reverse	Hypothetical protein
ORF34	15819	16310	492	reverse	Hypothetical protein
ORF35	16312	16815	504	reverse	Hypothetical protein
ORF36	16833	17114	282	reverse	Hypothetical protein
ORF37	17116	17607	492	reverse	Hypothetical protein
ORF38	17614	17886	273	reverse	Hypothetical protein
ORF39	18211	18489	279	reverse	Hypothetical protein
ORF40	18621	18893	273	forward	Hypothetical protein
ORF41	18883	19143	261	reverse	Hypothetical protein
ORF42	19275	19544	270	reverse	Hypothetical protein

ORF43	19576	20238	663	reverse	Hypothetical protein
ORF44	20235	20450	216	reverse	Hypothetical protein
ORF45	20453	21103	651	reverse	Hypothetical protein
ORF46	21100	21627	528	reverse	Hypothetical protein
ORF47	21617	21943	327	reverse	Hypothetical protein
ORF48	21933	22127	195	reverse	Hypothetical protein
ORF49	22349	22540	192	reverse	Hypothetical protein
ORF50	22540	23028	489	reverse	Hypothetical protein
ORF51	23126	23482	357	reverse	Hypothetical protein
ORF52	23482	24684	1203	reverse	Hypothetical protein
ORF53	24728	24961	234	reverse	Hypothetical protein
ORF54	24951	27596	2646	reverse	Hypothetical protein
ORF55	28420	29502	1083	forward	Hypothetical protein
ORF56	29499	32120	2622	forward	Hypothetical protein
ORF57	32187	32435	249	forward	Hypothetical protein
ORF58	32445	34034	1590	forward	**Helicase**
ORF59	34031	34768	738	forward	Hypothetical protein
ORF60	34780	35904	1125	forward	**Nuclease activity**
ORF61	35915	36361	447	forward	Hypothetical protein
ORF62	36416	37003	588	forward	Hypothetical protein
ORF63	36981	37802	822	forward	Hypothetical protein
ORF64	37807	38370	564	forward	**Chaperone**
ORF65	38384	40072	1689	forward	**Chaperone**
ORF66	40221	40373	153	forward	Hypothetical protein
ORF67	40409	43393	2985	forward	**DNA polymerase**
ORF68	43583	44200	618	forward	Hypothetical protein
ORF69	44233	47292	3060	reverse	**Tail sheath**
ORF70	47362	47493	132	reverse	Hypothetical protein
ORF71	47608	50403	2796	reverse	Hypothetical protein
ORF72	50535	52541	2007	reverse	**Helicase**
ORF73	52704	53246	543	reverse	**Dihidrofolate reductase**
ORF74	53331	54722	1392	reverse	**Helicase/primase**
ORF75	54739	55476	738	reverse	Hypothetical protein
ORF76	55593	57365	1773	reverse	Hypothetical protein
ORF77	57375	58094	720	reverse	Hypothetical protein
ORF78	58097	58258	162	reverse	**Chaperone**
ORF79	58275	59636	1362	reverse	**Helicase**
ORF80	59691	60998	1308	reverse	Hypothetical protein
ORF81	61040	61273	234	forward	Hypothetical protein
ORF82	61275	61955	681	reverse	Hypothetical protein
ORF83	62001	62615	615	reverse	Hypothetical protein
ORF84	62619	63272	654	reverse	**DNA end protecting protein**
ORF85	63316	63699	384	forward	Hypothetical protein
ORF86	63758	64360	603	reverse	Hypothetical protein
ORF87	64320	64523	204	reverse	Hypothetical protein
ORF88	64532	64810	279	reverse	Hypothetical protein
ORF89	64820	65260	441	reverse	Hypothetical protein

ORF90	65321	65791	471	reverse	Hypothetical protein
ORF91	65805	66467	663	reverse	Hypothetical protein
ORF92	66471	67625	1155	reverse	**Thymidylate synthetase**
ORF93	67707	68411	705	reverse	Hypothetical protein
ORF94	68586	69206	621	reverse	Hypothetical protein
ORF95	69188	70024	837	reverse	**Guanylate kinase**
ORF96	70098	71411	1314	reverse	Hypothetical protein
ORF97	71500	72132	633	forward	**Hydrolase**
ORF98	72167	72355	189	forward	Hypothetical protein
ORF99	72339	72542	204	reverse	Hypothetical protein
ORF100	72549	72845	297	reverse	Hypothetical protein
ORF101	72845	73624	780	reverse	**Baseplate protein**
ORF102	73699	75603	1905	forward	Hypothetical protein
ORF103	75645	77216	1572	reverse	**Baseplate wedge protein**
ORF104	77246	78010	765	reverse	**Endonuclease**
ORF105	78049	80061	2013	forward	Hypothetical protein
ORF106	80063	83206	3144	forward	Hypothetical protein
ORF107	83270	85345	2076	forward	Hypothetical protein
ORF108	85417	86064	648	reverse	Hypothetical protein
ORF109	86100	86387	288	reverse	Hypothetical protein
ORF110	86395	86685	291	reverse	Hypothetical protein
ORF111	86688	86939	252	reverse	Hypothetical protein
ORF112	86943	87311	369	reverse	Hypothetical protein
ORF113	87413	87964	552	reverse	Hypothetical protein
ORF114	87964	88302	339	reverse	Hypothetical protein
ORF115	88389	91067	2679	forward	Hypothetical protein
ORF116	91070	91561	492	forward	**Head completion protein**
ORF117	91554	91925	372	reverse	Hypothetical protein
ORF118	91950	93131	1182	reverse	**DNA primase/helicase**
ORF119	93234	94436	1203	reverse	Hypothetical protein
ORF120	94589	94993	405	reverse	Hypothetical protein
ORF121	95038	95433	396	reverse	Hypothetical protein
ORF122	95698	96267	570	reverse	Hypothetical protein
ORF123	96272	99046	2775	reverse	**Nudix hydrolase**
ORF124	99059	99814	756	reverse	Hypothetical protein
ORF125	99826	100794	969	reverse	Hypothetical protein
ORF126	100791	101453	663	reverse	Hypothetical protein
ORF127	102287	102688	402	forward	Hypothetical protein
ORF128	102636	104255	1620	forward	Hypothetical protein
ORF129	104308	104769	462	forward	Hypothetical protein
ORF130	104766	105500	735	forward	Hypothetical protein
ORF131	105670	105957	288	forward	**DNA binding protein**
ORF132	106029	106430	402	reverse	Hypothetical protein
ORF133	106442	109003	2562	reverse	Hypothetical protein
ORF134	109068	109832	765	forward	**Neck protein**
ORF135	109839	110087	249	reverse	Hypothetical protein
ORF136	110089	111072	984	reverse	**Sliding clamp protein**

ORF137	111157	111639	483	reverse	**Peptidase**
ORF138	111742	112755	1014	forward	**Ribonucleoside reductase alpha**
ORF139	112888	113595	708	forward	Hypothetical protein
ORF140	113692	117906	4215	forward	**Prohead scaffold**
ORF141	118051	119394	1344	forward	**Adenylosuccinate synthetase**
ORF142	119418	121289	1872	forward	**Terminase large subunit**
ORF143	121438	123144	1707	forward	**Ribonucleoside reductase beta**
ORF144	123173	123388	216	forward	Hypothetical protein
ORF145	123471	125399	1929	forward	Hypothetical protein
ORF146	125545	127206	1662	forward	**Major capsid protein**
ORF147	127316	127843	528	reverse	**Baseplate wedge protein**
ORF148	127955	129646	1692	reverse	Hypothetical protein
ORF149	129735	131090	1356	forward	**Adenylosuccinate lyase**
ORF150	131087	131665	579	reverse	Hypothetical protein
ORF151	131717	132250	534	forward	Hypothetical protein
ORF152	132257	133225	969	forward	Hypothetical protein
ORF153	133276	136560	3285	reverse	Hypothetical protein
ORF154	136761	137570	810	forward	Hypothetical protein
ORF155	137610	138587	978	forward	Hypothetical protein
ORF156	138580	138750	171	forward	Hypothetical protein
ORF157	138798	139484	687	forward	Hypothetical protein
ORF158	139481	139900	420	reverse	Hypothetical protein
ORF159	139939	140550	612	reverse	Hypothetical protein
ORF160	140555	141133	579	reverse	**Endonuclease**
ORF161	141133	143094	1962	reverse	**DNA ligase**
ORF162	143181	143567	387	reverse	**Endonuclease**
ORF163	143571	144095	525	reverse	**Glycoside hydrolase**
ORF164	144189	144629	441	reverse	Hypothetical protein
ORF165	144633	145253	621	reverse	Hypothetical protein
ORF166	145241	145546	306	reverse	Hypothetical protein
ORF167	145284	145433	150	forward	Hypothetical protein
ORF168	145461	145643	183	forward	Hypothetical protein
ORF169	145664	146389	726	reverse	Hypothetical protein
ORF170	146422	147570	1149	reverse	Hypothetical protein
ORF171	147563	147745	183	reverse	Hypothetical protein
ORF172	147757	151512	3756	reverse	Hypothetical protein
ORF173	151538	151645	108	reverse	Hypothetical protein
ORF174	151666	151965	300	reverse	Hypothetical protein
ORF175	151969	153396	1428	reverse	**Leucine rich repeat protein**
ORF176	153401	155008	1608	reverse	**Leucine rich repeat protein**
ORF177	155023	159075	4053	reverse	Hypothetical protein
ORF178	159186	159737	552	reverse	Hypothetical protein
ORF179	159766	160479	714	reverse	Hypothetical protein
ORF180	160470	160751	282	reverse	Hypothetical protein
ORF181	160820	161338	519	reverse	Hypothetical protein
ORF182	161494	161748	255	reverse	Hypothetical protein
ORF183	161748	162197	450	reverse	Hypothetical protein

ORF184	162172	162672	501	reverse	Hypothetical protein
ORF185	162706	163071	366	reverse	Hypothetical protein
ORF186	163077	163442	366	reverse	Hypothetical protein
ORF187	163461	163820	360	reverse	Hypothetical protein
ORF188	163829	164506	678	reverse	Hypothetical protein
ORF189	164503	165036	534	reverse	Hypothetical protein
ORF190	165020	165349	330	reverse	Hypothetical protein
ORF191	165367	165699	333	reverse	Hypothetical protein
ORF192	165701	166381	681	reverse	Hypothetical protein
ORF193	166493	167233	741	reverse	Hypothetical protein
ORF194	167243	167563	321	reverse	Hypothetical protein
ORF195	167562	167711	150	forward	Hypothetical protein

APPENDIX 4: PLAQUE MORPHOLOGIES ON OTHER HOSTS OTHER THAN B330

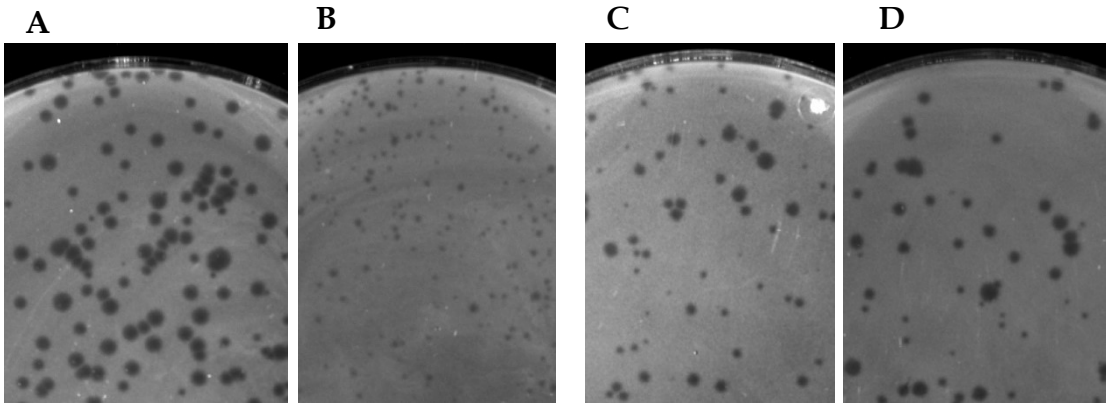

Appendix 4. Plaque morphologies of FLiP and FLiP-2 plated with different hosts. A. are the plaques of FLiP on B114 B. are plaques of FLiP-2 on B114 C. are plaques of FLiP on B167 D. are plaques of FLiP-2 on B167.

APPENDIX 5: EARLY FLIP ONE STEP GROWTH CURVE

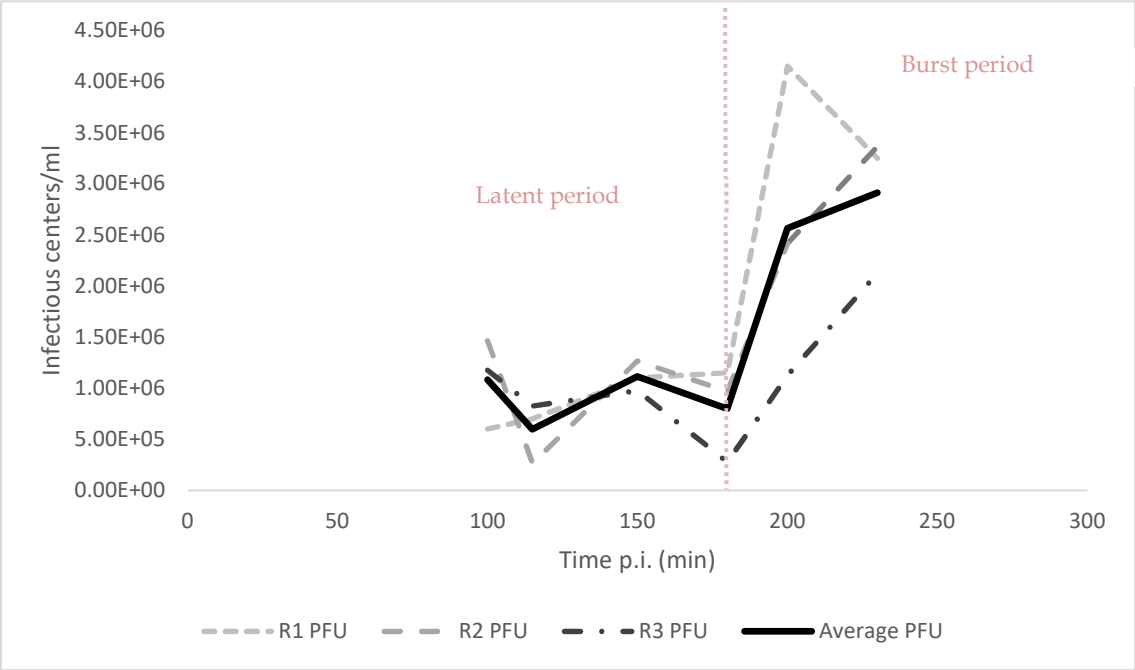

Appendix 5. One step growth curve of FLiP with B330 host showing the timing and magnitude of titre increase. The X-axis shows the time in minutes post infection, the left Y-axis corresponds to the increase in bacteriophage titers measured in infective centers per ml. This was the test one step growth curve performed prior to the real tests with longer sampling periods.